Contents lists available at ScienceDirect

Chemical Geology

journal homepage: www.elsevier.com/locate/chemgeo





A systematic evaluation of titanite reference materials for optimizing trace element and U—Pb analysis by LA-ICP-MS

Anca Barla ^{a,b,*}, Antoine Triantafyllou ^c, Mihai N. Ducea ^{b,a}, Gilby Jepson ^{a,e}, William McClelland ^d, Dominique Giesler ^a, George E. Gehrels ^a, Clémentine Fellah ^c

- ^a Department of Geosciences, University of Arizona, Tucson, AZ 85721, USA
- ^b Faculty of Geology and Geophysics, University of Bucharest, Bucharest, 010040, Romania
- c Lyon Geology Laboratory Earth, Planets and Environment (LGL-TPE), Université Lyon 1, ENS de Lyon, CNRS, UMR, Villeurbanne 5276, France
- ^d Department of Earth & Environmental Sciences, University of Iowa, Iowa City, IA 52242, USA
- e School of Geosciences, University of Oklahoma, Norman, OK 73019, USA

ARTICLE INFO

Editor: Balz Kamber

Keywords:
Titanite
Trace elements
Matrix-matched reference materials
LA-HR-ICP-MS
Non-radiogenic Pb

ABSTRACT

Titanite (CaTiSiO₅) is a commonly occurring and versatile accessory mineral with broad applications in petrochronology. In situ U-Pb and trace element analyses via SIMS and LA-ICPMS are routinely performed using a matrix-matched reference material for U-Pb and standard glasses (non-matrix matched reference material) for elemental abundance determination. We report U-Pb isotopic ratios and major and trace element concentrations for three titanite samples (Ecstall, McClure and FCT) which are commonly used as reference materials in petrochronology studies. In addition, we characterize two new samples which can potentially serve as matrixmatched reference materials for titanite trace element geochemistry (BLR-2 and BRA-1). Based on electron microprobe analysis, samples BLR-1 and BLR-2 are homogeneous and suitable for use as a primary reference material for trace element concentrations. Whereas Ecstall, McClure, and FCT titanite reference materials show high intra-grain heterogeneity, yielding relative standard deviations for most trace elements between 5% and 40%, with higher standard deviations for U of 70% for Ecstall (n = 26), 265% for McClure (n = 22), and 202% for FCT (n = 26). Therefore, we suggest that these grains are unsuited to serve as reference materials for trace element quantification. The BRA-1 titanite has low trace element concentrations and is chemically heterogeneous (total REE abundances of 40 ppm for the rim and 95 ppm for the core of the grain), thus is not suitable for standardization of chemical composition using LA-ICPMS. It is commonly asserted that a matrix-matched standardization provides a more robust downhole fractionation correction compared to a non-matrix matched standardization. However, it remains unclear which standardization approach (matrix-matched vs non-matrix matched/glass) is more accurate for titanite trace element quantification. To resolve this, we tested several standardization approaches for trace element quantification, comparing matrix-matched (BLR-1) and nonmatrix-matched (NIST612) standardizations with different internal elemental standards (IES; Ca, Si and Ti) and without internal standardization (semi-quantitative). To provide an independent constraint on the accuracy of the various trace element standardization techniques we compared results to trace element concentrations obtained via solution O-ICPMS on crushed BLR-2 and BRA-1 aliquots. The matrix-matched standardization using Si as the IES yields the best reproducibility of trace element concentrations followed by the matrix-matched reduction using Ti as the IES. Moreover, the matrix-matched semi-quantitative correction yielded the lowest weighted percentage of difference compared to reference trace composition quantified by solution ICPMS. Finally, in this contribution we also benchmark sampling-size for precise U-Pb dating of common-Pb rich phases like titanite.

^{*} Corresponding author at: Department of Geosciences, University of Arizona, Tucson, AZ, 85721, USA. *E-mail address:* ancabarla@arizona.edu (A. Barla).

1. Introduction

Titanite is a commonly occurring accessory mineral found in igneous and metamorphic rocks (e.g., Smith, 1970; Nakada, 1991). Its composition and crystal structure allow the incorporation of a significant amount of U, Pb, Th and other trace elements (i.e., High Field Strength Elements and Rare Earth Elements), making it a robust candidate for petrochronological studies (e.g., Kohn, 2017; Scibiorski and Cawood, 2022). The combination of in-situ U-Pb isotope and trace elements analysis in titanite and other U-bearing accessory mineral phases has undergone rapid improvement in precision and accuracy over the last decade. Some studies decouple the isotopic measurement from trace element analysis using Laser Ablation-Inductively Coupled Plasma-Mass Spectrometry (LA-ICP-MS), Thermal Ionization Mass Spectrometry (TIMS) sensu lato, or Secondary Ion Mass Spectrometry (SIMS) for U-Pb ratio determination and LA-ICP-MS or electron microprobe (EMP) analysis close to the previously ablated areas, for trace elements concentrations (e.g., Kylander-Clark et al., 2013; Glorie et al., 2019). More recently, workers tend to combine the analysis of U-Pb ratios and elemental concentrations from the same analyte volume, thus allowing direct linking between age and chemistry using quadrupole ICP-MS (e. g., Li et al., 2000), SIMS (e.g., Mcclelland et al., 2009) or Laser Ablation Split Stream (LASS) ICP-MS (Chen et al., 2010; Kylander-Clark et al., 2013; Stearns et al., 2016) or LA-High Resolution-ICP-MS (HR, Chapman et al., 2016; this study). Regarding U-Pb dating, several authors showed that titanite could retain its radiogenic Pb content over long-term and high-grade heating events (650–700 °C, see e.g., Kohn and Corrie, 2011; Gao et al., 2012 or even higher than 750 °C; see Spencer et al., 2013; Kohn, 2017; Smye et al., 2018) when compared to laboratory diffusion studies (e.g., Cherniak, 1993). The high closure temperature compatible with slower Pb diffusion in titanite, and the fact that U-Pb systematics are strongly influenced by metamorphic growth (Frost et al., 2001), make titanite a powerful and complementary approach in dating both igneous events and also successive metamorphic - and deformation events (Essex and Gromet, 2000; Papapavlou et al., 2018; Walters et al., 2022; Moser et al., 2022), mineral deposits (Pan et al., 2018; Liu et al., 2022) and hydrothermal overprinting (Song et al., 2019; Hart-Madigan et al., 2020).

Obtaining accurate U-Pb ages in titanite is hindered by the presence of high and variable non-radiogenic Pb/radiogenic Pb ratios (e.g., Frost et al., 2001; Aleinikoff et al., 2002; Kirkland et al., 2018), which requires a non-radiogenic Pb correction of the raw U-Pb isotopic dataset (see Storey et al., 2006; Chew et al., 2014; Jepson et al., 2021 for apatite nonradiogenic Pb correction). One approach is to combine uncorrected U-Pb analyses from a suite of cogenetic titanite grains with varying abundances of non-radiogenic Pb. Based on the spread of cogenetic titanites along a shared isotopic evolution line, U-Pb ages can be determined either by using the lower intercept age in a Tera-Wasserburg diagram or as a weighted average of ²⁰⁷Pb-corrected ages using the non-radiogenic Pb composition from the upper intercept (Simonetti et al., 2006; Chew et al., 2011 similarly for apatite U-Pb dating). Therefore, having spread in the uncorrected U-Pb data, i.e., the variable incorporation of nonradiogenic Pb, is key in calculating precise U-Pb age (Kirkland et al., 2018). Whereas the variation in non-radiogenic Pb is mainly dependent on the sample, multiple cogenetic grains and multiple spots can increase the chance of constraining a non-radiogenic Pb isotope line. Ideally, this information should be assessed during a LA-ICP-MS session to know how many analyses are required to constrain non-radiogenic Pb composition and ultimately, estimate a precise and accurate Pb-corrected age. Presently, the relationship among the amount of non-radiogenic Pb in titanite, the number of analyses and its effect on age accuracy and precision is not explored.

Titanite trace element concentrations are able to document thermobarometry and fingerprint petrogenetic conditions. Ti and Zr content can substitute between cogenetic titanite, rutile and zircon (Ferry and Watson, 2007; Hayden et al., 2008; Tomkins et al., 2007; Zack et al.,

2004). The substitution of Ti and Zr is regulated by temperature, making titanite a useful geo-thermometer (Hayden et al., 2008; Timms et al., 2011), and has been successfully applied to understanding the thermal evolution of various tectonic systems (Stearns et al., 2015; Schwartz et al., 2016; Mottram et al., 2019). The rare earth element (REE) signature of titanite has also been found to distinguish between different generations of mineral growth (Scibiorski et al., 2019) or to reveal the petrogenetic conditions during their crystallization (e.g., Mazdab, 2009; Gao et al., 2011; Olierook et al., 2019). Central to titanites petrological utility is the accurate determination of trace element concentrations. It is widely accepted that using a matrix-matched reference material more reliably quantifies trace element concentrations using LA-ICP-MS (Miliszkiewicz et al., 2015; Spandler et al., 2016). Despite this, there are still numerous studies that use reference glass material as primary standards (e.g., NIST610; NIST612; BHVO-2). Further, after trace element measurements there remain several methods for standardizing the raw data to a final concentration. The most common standardization technique is using Ca, Si or Ti, assumed as either stoichiometric or determined from EMP analyses, as an internal standard (e.g., Tiepolo et al., 2002, Stearns et al., 2016, Papapavlou et al., 2018, Cioffi et al., 2019, Kirkland et al., 2020). However, some studies employ the semi-quantitative technique relative to a matrix-matched standard which requires no internal standardization (e.g., Ubide et al., 2015). Moreover, some studies apply a sum normalization calibration method for trace elements quantification (e.g., Liu et al., 2008; He et al., 2013). This method does not require an internal elemental standard but relies on analysis of as many elements as possible. Due to the variety of approaches, the effect of using matrix-matched versus non-matrix-matched standardization on trace element concentrations remains poorly documented for Ti-rich mineral phases, despite its importance for producing consistent petrochronological interpretations.

The aim of this study is three-fold: (i) Provide a new detailed characterization of major and trace element composition for commonly used titanite reference materials (i.e., Bear Lake Ridge, Ecstall, McClure, BRA-1 and Fish Canyon Tuff titanites). (ii) Quantify the effect of using matrixmatched (BLR-1 titanite) versus non-matrix matched (NIST612 glass) as primary standards for quantifying titanite trace element concentrations. Here, we explore the impact of applying different data reduction schemes, internal standardization with Ca vs Si vs Ti as internal elemental standards and semi-quantitative reduction without internal standardization on the final titanite trace element concentration. (iii) To suggest benchmarks and discuss limitations for U-Pb analysis on nonradiogenic Pb rich titanite. Specifically, a minimum number of U-Pb analyses, F207%, and expected accuracy and precision based on statistical bootstrap analysis. Finally, we present Sr isotope ratios via TIMS for BLR-2 and BRA-1 titanite, to further characterize these grains as reference materials for additional isotopic analyses (see Supplementary Materials Doc. S1).

2. Material and methods

2.1. Sample description and preparation

In this study, we characterized three readily available titanite U-Pb standards (Ecstall, McClure, FCT) and one commonly used titanite U-Pb standard (BLR-1), and present two new titanite U-Pb and trace element reference materials (BLR-2 and BRA-1). Bear Lake Road titanite (BLR-1; 1047.1 ± 0.4 Ma, Aleinikoff et al., 2007; Spencer et al., 2013, Stearns et al., 2016) is a compositionally homogeneous metamorphic megacrystal (10^4 µm) collected from Bear Lake Diggings, Ontario (Canada). The BLR-1 titanite occurs in calcite veins of controversial origin within the highly deformed Central Metasedimentary Belt of the Grenville Province (Hewitt and Thomson, 1956). The BLR-2 titanite is a centimetric metamorphic grain weighting \sim 6 g, collected from the same location as BLR-1. The BLR-1 titanite has reported isotopic values of: $^{206}\text{Pb}/^{238}\text{U} = 0.176257 \pm 0.093333$, $^{207}\text{Pb}/^{235}\text{U} = 1.805717 \pm$

0.125000, $^{207}\text{Pb}/^{206}\text{Pb} = 0.074303 \pm 0.073333$ (Aleinikoff et al., 2007), and Pb, Th and U concentrations of 19.7 ppm, 186.0 ppm, and 300.0 ppm, respectively (Mazdab, 2009). Ecstall titanite is a small (typically 300 µm long) igneous titanite from the Ecstall pluton in British Columbia (zircon U-Pb age of 91.5 \pm 1.0 Ma; Butler et al., 2002). The Ecstall pluton is a large granitic body flanking the western edge of the Coast Mountains and is composed of hornblende quartz diorite and granodiorite (Hutchison, 1982). The BRA-1 grain is a large pluri-centimetric (~3 cm long) yellowish titanite grain from Brazil. McClure titanites are small (typically 300 µm long) igneous grains extracted from the syenite in the McClure Mountains in Colorado, USA. The McClure Mountains are an alkalic complex, a syenite body intrudes cumulates of olivine, pyroxene and plagioclase (Alexander Jr, 1979; Olson et al., 1977). Alongside its major mineralogical composition (plagioclase, potassium feldspar, clinopyroxene, hornblende, clinopyroxene), the syenite body contains abundant accessory minerals such as apatite and titanite (e.g., Schoene and Bowring, 2006). Previous geochronological studies on McClure titanite revealed a Pbcm-corrected 207 Pb/ 235 U age of 523.26 \pm 1.27 Ma (Schoene and Bowring, 2006). The FCT titanites are 500 µm long orange grains from the Fish Canyon Tuff, a quartz latite ash-flow in the San Juan Mountains in Colorado. The Fish Canyon Tuff is an Oligocene large volume ash-flow contains abundant hornblende, biotite, plagioclase, sanidine, quartz, titanite and ilmenite and is chemically and mineralogically homogeneous (Whitney et al., 1985). Schmitz and Bowring (2001) determined the Pbcm-corrected $^{207}\text{Pb}/^{235}\text{U}$ weighted mean age of FCT titanite to be 28.87 \pm 0.50 Ma.

2.2. SEM analyses

Scanning Electron Microscope (SEM) analyses were performed at the Lyon Geology Laboratory: Earth, Planets, Environment (Lyon, France). Mineral separates of BLR-1, BLR-2, Ecstall, McClure, BRA-1 and FCT titanites were mounted in epoxy resin, polished to half grain thickness, and coated with a 10 nm thick carbon layer to reduce charging in the Scanning Electron Microscope (SEM). These samples were analyzed in a high vacuum by energy-dispersive X-ray (EDX)-SEM (Zeiss Supra 55VP with Aztec Oxford System - DDI detector X-Max) operated at 5 kV for secondary electron (SE) and 15 kV for EDX analyses, element mapping and backscattered electron (BSE) imaging. The BLR-1 and Ecstall titanite grains do not show mineral inclusions. The McClure titanite grains show occasional plagioclase grains along the rims (Fig. 1). The FCT titanites contain several zircon inclusions (< 50 µm) and small alkali feldspar grains along the rims. The BLR-2 metamorphic titanite crystal contains few small inclusions of iron oxides (< 10 μm), Nb-rich rutile and quartz $(<70 \mu m)$. These inclusions are very rare and easy to avoid using BSE or reflected light images.

2.3. Electron microprobe analyses

Electron Microprobe (EMP) analyses were conducted at the Lunar and Planetary Laboratory (University of Arizona) using a CAMECA SX100 equipped with 5 WDS detectors. The instrument was calibrated with natural and synthetic standards; matrix corrections were made using the CITZAF and PaP algorithms. EMP ran at two distinct conditions: the first one at 20 keV of voltage and 20 nA of current at a beam size of 1 μm for SiO2, Na2O, Al2O3, TiO2, K2O, CaO, FeOT, Cr2O3, MnO and F and the second one at 20 keV and 299 nA at a beam size of 5 μm for lower concentrated elements, including Zr, Sr, Nb, Ce, Nd, Mg, Y, Th and U. Mineral compositions, detection limits (LOD), and detailed analytical and standardization conditions are available in Supplementary Materials Table S1.

2.4. Whole-grain analyses using solution-ICP-MS

Solution ICP-MS analyses were performed at the Geosciences Department - University of Arizona (Tucson, AZ, USA). Two titanite grains (BLR-2 and BRA-1) were selected for solution ICP-MS because of their large size and availability. Each large grain was micro-sampled from core to rim using a Micromill instrument (from NewWave-Merchantek with diamond drill bits from Brasseler Instrument; Ducea et al., 2003). For whole-grain trace element analysis, about 150–100 mg of powder was digested in a Teflon beaker in a tunnel oven with LiBO2-Li2B4O7 according to the protocols of the French national research facility SARM-**CRPG** (https://sarm.cnrs.fr/index.html/qui-sommes-nous/parc-anal ytique-2/). The resulting solutions were dried, and the residues were completely redissolved in HNO3 acid. The trace elements were analyzed using an iCapQ ICP-MS (Thermofisher). During the analytical session, As, Ba, Be, Bi, Cd, Ce, Co, Cr, Cs, Cu, Dy, Er, Eu, Ga, Gd, Ge, Hf, Ho, La, Lu, Mo, Nb, Nd, Ni, Pb, Pr, Rb, Sb, Sm, Sn, Sr, Ta, Tb, Th, Tm, U, V, W, Y, Yb, Zn, Zr elemental concentrations were measured. All the analyses were quality-checked with one reference sample out of every ten and internal reference materials. The accuracy is within 5% of the certified values and typically within <3% for most elements analyzed. For detailed analytical procedure, see Carignan et al. (2001).

2.5. LA-HR-ICP-MS analyses

The chemical and isotopic analyses in this study were performed at the Arizona LaserChron Center (www.laserchron.org), an NSF Community Facility housed in the Department of Geosciences at the University of Arizona (Tucson, AZ, USA). The isotopic abundances of U-Th-Pb and trace and REE on titanite were determined simultaneously using a Thermo Element2 HR ICP-MS coupled to Photon Machines Analyte G2 excimer laser equipped with HelEX low-volume cells. A standardunknown bracketing was performed during each analytical run which provides a robust correction of the downhole elemental fractionation during ablation. The pre-ablation run (cleaning shots) were performed by three shots at $65 \mu m$ spot size per location and on-sample laser fluence of 5.54 J/cm². The ablation was carried out with a 30 μm spot size, and a laser fluence of 5.56 J/cm² at 7 Hz. The acquisition mode employed was time-resolved analysis and the detector counting modes were in pulse-counting mode for signals below 5×10^6 counts per second (cps) and analog mode (i.e., volts) for signals above 5×10^6 cps. The analog mode measurements are converted to cps using the analog conversion factor (ACF, Pullen et al., 2018). Each analytical run consisted of 10 s of background acquisition, 45 s of ablation and 10 s of washout, leading to 73 rows of data per analysis. Six jumps in magnet setting were used during each scan. He-Ar mixture was used as carrier gas, and plasma torch conditions were optimized so that UO/U ratios were below 0.7%. The HelEx-2 cells allow for fast transport of the analyte to the plasma, and thus, culminating in a fast return to background values after the ablation (Pullen et al., 2018). The LA-HR-ICP-MS instrumentation and acquisition parameters used in this study are summarized in Table 1.

During the typical analytical run the following elemental concentrations were quantified: $^{27}\mathrm{Al},~^{30}\mathrm{Si},~^{42}\mathrm{Ca},~^{49}\mathrm{Ti},~^{55}\mathrm{Mn},~^{57}\mathrm{Fe},~^{85}\mathrm{Rb},~^{86,87,88}\mathrm{Sr},~^{89}\mathrm{Y},~^{90}\mathrm{Zr},~^{91}\mathrm{Zr},~^{93}\mathrm{Nb},~^{97}\mathrm{Mo},~^{139}\mathrm{La},~^{140}\mathrm{Ce},~^{141}\mathrm{Pr},~^{146}\mathrm{Nd},~^{147}\mathrm{Sm},~^{151}\mathrm{Eu},^{157}\mathrm{Gd},~^{159}\mathrm{Tb},~^{163}\mathrm{Dy},~^{165}\mathrm{Ho},~^{166}\mathrm{Er},~^{169}\mathrm{Tm},~^{174}\mathrm{Yb},~^{175}\mathrm{Lu},~^{178}\mathrm{Hf},~^{181}\mathrm{Ta},~^{183}\mathrm{W},~^{204,206,207,208}\mathrm{pb},~^{232}\mathrm{Th}$ and $^{238}\mathrm{U}.$ Most of the elements were measured for 0.01 s and the dwell times were increased to 0.02 s for elements which are commonly present in low concentrations in titanite (Tm, Yb, Lu). The mass spectra were reduced using Iolite software version 3.2 (Paton et al., 2011).

3. Results

3.1. Electron microprobe data and grain homogeneity

All EMP data are summarized in Table 2 and Fig. 2. Titanite sample BLR-1 is a homogenous grain, as reflected in the major and trace element composition (Table 2). Most elements show a relative standard deviation (RSD) of <15% (N=19). A higher RSD is displayed by F (19%), K₂O (112%), Cr (34%), Mn (17%) and U (72%).

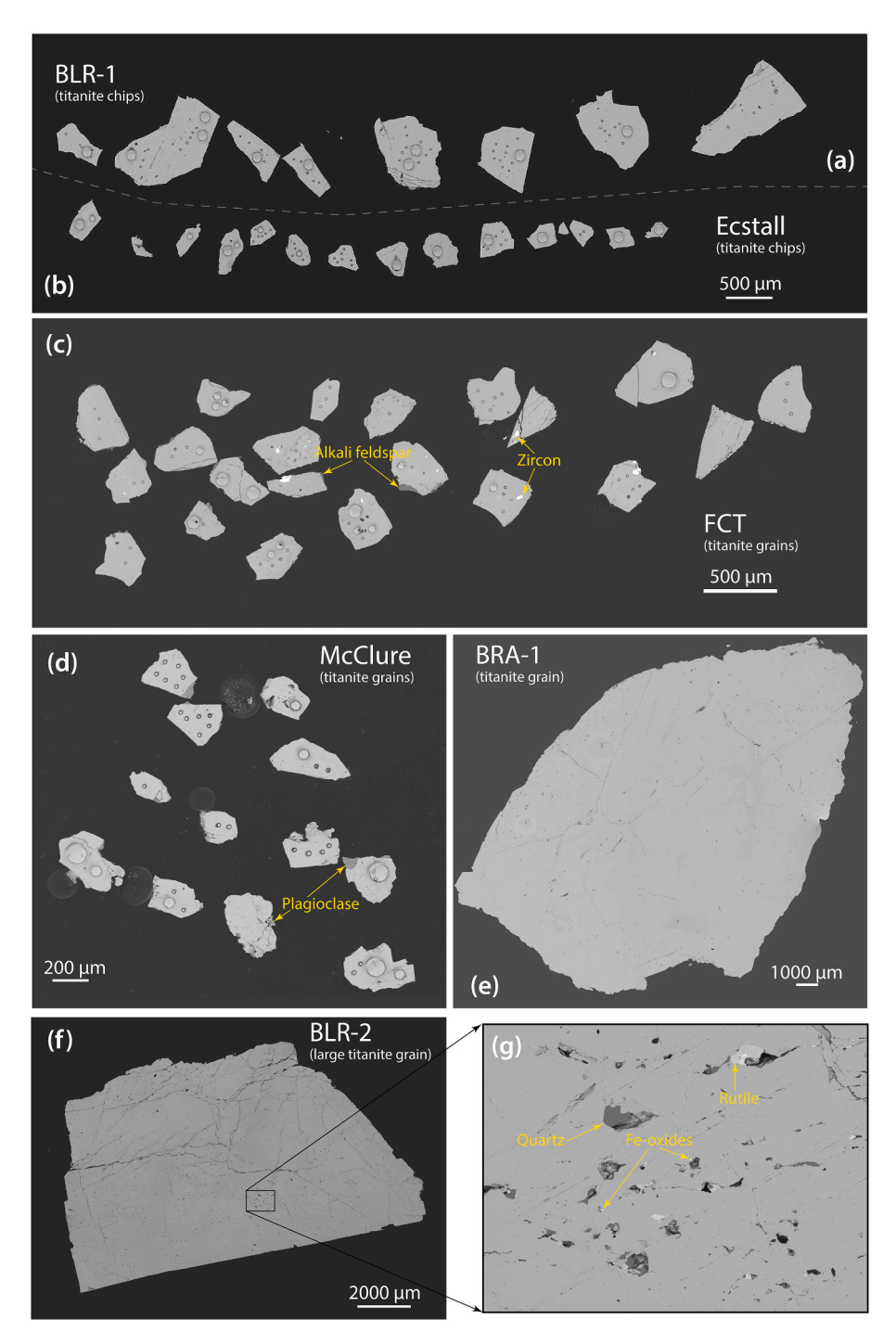


Fig. 1. BSE images of titanite grains (a) BLR-1, (b) Ecstall, (c) Fish Canyon Tuff, (d) McClure, (e) BRA-1, (f) BLR-2, (g) detail of BLR-2 titanite grain. Yellow arrows and labels indicate the mineral inclusions observed during EDX analysis. (For interpretation of the references to colour in this figure legend, the reader is referred to the web version of this article.)

Similar to BLR-1, BLR-2 grain shows chemical homogeneity, with most of the analyzed elements having RSD <15% (n=55). Elements such as Cr, Mn, and Th have higher RSD, between 15% and 35%. Potassium and uranium are less homogeneous within the BLR-2 crystal structure, with RSD of 153% and 105%, respectively. The Ecstall titanite is homogeneous in major elements (Al₂O₃, SiO₂, TiO₂, CaO, Cr₂O₃, FeO) with RSD < 15% (n=26). Intra-sample distribution of Zr shows an RSD of 39%, with a mean of 366 ppm. The Ecstall titanite has high and variable Y (mean: 1096 ppm, RSD: 25%) and U (mean: 157 ppm, RSD: 70%) elemental concentrations. The McClure titanite is homogeneous in many of the analyzed elements (RSD < 15%; n=22) containing elevated

Zr (mean: 3026 ppm, RSD: 10%) and Y (mean 596 ppm, RSD: 13%) and low and variable U content (mean: 13, RSD: 265%). The FCT titanite is chemically homogeneous yielding an RSD of $<\!15\%$ for most of the measured elemental concentrations. Moreover, the FCT titanite contains high Y contents (mean: 4369 ppm). Core to rim transects on the McClure and FCT titanite grains also reveal low RSD for Y and Ce ($<\!10\%$ for McClure and $<\!3\%$ for FCT), and variable U concentrations (RSD of 201% for McClure and 73% for FCT). The BRA-1 titanite contains variable mass fractions of most trace elements of interest (e.g., Zr, Y, U, Th), with Ce behaving more homogeneously on an intra-sample level (RSD: 17%; n=71).

Table 1LA-HR-ICPMS Instrumentation and acquisition parameters.

Photon analyte G2 with Thyratron 193 nm excimer laser
HelEx
96.2
7
Thermo Element2 HR-ICPMS
16
0.8
1250
Both pulse-counting and analog mode
Time resolved analysis
3 shot counts, 65 μm
325 shots, 30 μm
5.56
45 s
10 s
10 s
²⁷ Al, ³⁰ Si, ⁴² Ca, ⁴⁹ Ti, ⁵⁵ Mn, ⁵⁷ Fe, ⁸⁵ Rb, ⁸⁶ Sr, ⁸⁷ Sr, ⁸⁸ Sr,
⁸⁹ Y, ⁹⁰ Zr, ⁹¹ Zr, ⁹³ Nb, ⁹⁷ Mo, ¹³⁹ La, ¹⁴⁰ Ce, ¹⁴¹ Pr, ¹⁴⁶ Nd,
¹⁴⁷ Sm, ¹⁵¹ Eu, ¹⁵⁷ Gd, ¹⁵⁹ Tb, ¹⁶³ Dy, ¹⁶⁵ Ho, ¹⁶⁶ Er, ¹⁶⁹ Tm,
¹⁷⁴ Yb, ¹⁷⁵ Lu, ¹⁸¹ Ta, ¹⁸³ W, ²⁰² Hg, ²⁰⁴ Pb, ²⁰⁶ Pb, ²⁰⁷ Pb,
²⁰⁸ Pb, ²³² Th, ²³⁸ U
0.01 s for most of the elements, 0.02 s for Tm, Yb, Lu
BLR-1, NIST612

3.2. Whole-grain composition using solution ICP-MS

Solution ICP-MS data for BLR-2 and BRA-1 titanite are presented in Table 3 and the REE spider diagram for BLR-2 is shown in Fig. 4. The BLR-2 titanite has high Zr (1299.28 ppm), La (358.69 ppm), U (105.34 ppm) and Y (555.22 ppm) mean concentrations. The normalized REE trend for BLR-2 titanite shows a flat light REE (LREE) trend ([La/Sm]_N = 0.89) and a slight enrichment in LREE and medium REE (MREE) relative to heavy REE (HREE), with a [La/Yb]_N ratio of 4.93 and a [Dv/Yb]_N value of 2.01. Moreover, BLR-2 titanite exhibits a negative Eu anomaly (referred to as Eu/Eu*) of 0.56. Comparatively, BRA-1 titanite shows low overall trace element concentrations, with mean values for Zr, U, La and Y of 29.81 ppm, 162.35 ppm, 0.90 ppm and 3.32 ppm, respectively. The BRA-1 titanite displays a steep depletion in LREE ([La/Sm]_N = 0.09)), an overall enrichment in HREE, with a [Dy/Yb]_N ratio of 0.76, and a small negative Eu/Eu* (0.84). Overall, the BRA-1 titanite has very low trace element concentrations typically <1 ppm for most trace elements investigated. Moreover, our solution ICPMS analyses on the two aliquots showed large concentration differences between the cores and the rims of the grain (Fig. S1).

3.3. LA-HR-ICP-MS analyses

3.3.1. Data reduction schemes (DRS)

The time-resolved U-Th-Pb and trace element data were reduced using Iolite v3 software (https://iolite-software.com; Paton et al., 2011, Petrus and Kamber, 2012). Within Iolite, the isotopic data for U-Pb dating were reduced using the VizualAge_UcomPbine Data Reduction Scheme (DRS; Chew et al., 2014). Titanite BLR-1 was used as the primary standard to correct for downhole fractionation and instrumental drift, and Ecstall titanite was used as a secondary reference material for data quality control.

For trace element data, four reduction protocols were applied to quantify the impact different DRS approaches can have on final elemental concentrations determined on titanite. The reduction schemes used were: The X_Trace_Elements DRS_semiquant with BLR-1 reference material as the primary standard for calculating semi-quantitative (SQ) elemental abundances, and X_Trace_Elements_IS separately using BLR-1 titanite and NIST612 glass to correct for instrumental drift and ⁴²Ca, ³⁰Si and ⁴⁹Ti EMP determined abundances, as the internal elemental standards (IES). Within the SQ DRS, the reference material analyses are integrated in the reduction protocol for calculating semi-quantitative elemental abundances (Paton et al., 2011). For the internally normalized calculations, the baseline-subtracted intensities are used to calculate the ratio of elements to the selected IES (Paton et al., 2011). Detailed trace element concentrations for the three DRS approaches are presented in Supplementary Table S3.

3.3.2. In situ U-Pb results

Analyses performed on titanite grains from the five samples (BLR-2, BRA-1, Ecstall, FCT, and McClure) show relatively high intra-sample variability in terms of U, Th and Pb concentrations (see Supplementary Materials Table S2). Median values are as follows: BLR-2: 196. 51 \pm 14.13 ppm U, 215.35 \pm 13.18 ppm Th, 23.06 \pm 1.49 ppm Pb; Ecstall: 453 \pm 26.33 ppm U, 428.38 \pm 38.44 ppm Th, 4.34 \pm 0.37 ppm Pb; BRA-1: 10.54 \pm 0.74 ppm U, 0.08 \pm 0.01 ppm Th, 0.97 \pm 0.07 ppm Pb; McClure: 79.23 \pm 5.53 ppm U, 156.14 \pm 8.36 ppm Th, 7.48 \pm 0.41 ppm Pb; FCT: 110.48 \pm 7.87 ppm U, 155.64 \pm 8.80 ppm Th, 1.11 \pm 0.08 ppm Pb.

The McClure titanite contained low concentrations of non-radiogenic Pb, whereas BLR-2, Ecstall, BRA-1, and FCT contain significant amounts of non-radiogenic Pb (common Pb or Pbcm). Isotopic ratios were corrected for downhole fractionation and instrumental drift (²³⁸U/²⁰⁶Pb and ²⁰⁷Pb/²⁰⁶Pb), plotted on a Tera-Wasserburg diagram and processed via linear regression to correct for Pbcm. The lower concordia intercept $(^{238}\mathrm{U}/^{206}\mathrm{Pb})$ represents an approximate age defined by the radiogenic Pb component in cases where the spread in the data allows for a precise regression. The y-intercept (207Pb/206Pb) represents the initial nonradiogenic Pb composition which can subsequently be used to apply a common 207 Pb correction to the 206 Pb/ 238 U ratio. Ages were calculated as the lower intercept (238 U/ 206 Pb) age on the concordia and as a weighted mean of the ²⁰⁷Pb-corrected ages for BLR-2, Ecstall, BRA-1 and FCT titanites. External errors have been propagated into the individual uncertainties of the ²⁰⁷Pb-corrected ages (Horstwood et al., 2016). For the McClure titanite, the concordia age and the uncorrected ²⁰⁶Pb/²³⁸U weighted mean age were determined. A summary of titanite U-Pb age results can be found in Table 4. Throughout this manuscript we use F207% (See Eqs (1) and (2) from Kirkland et al., 2018) as a measure of the non-radiogenic Pb content. The F207% is defined as the relative difference between the measured ²⁰⁶Pb/²³⁸Pb ratio and the ²⁰⁷Pb-corrected age recast as a concordant 206Pb/238Pb ratio (see Kirkland et al., 2018 for more details).

Concordant²⁰⁶Pb/²³⁸U ratio = EXP(0.000155125^{*207}corrected²³⁸U/
206
Pb age) - 1 (1)

$$F207\% = 100^* (1 - Concordant^{206}Pb/^{238}U ratio/^{206}Pb/^{238}U measured)$$
 (2)

Thirty-eight analyses on BLR-2 titanite define two distinct domains with variable amounts of non-radiogenic Pb, but the same initial Pb ratio $((^{207}\text{Pb}/^{206}\text{Pb})_o=1.000\pm0.140),$ defined by the upper intercept of the linear regression through these data on a Tera-Wasserburg diagram (Fig. 3). The most concordant domain has a F207% < 1%, whereas the other spot-population contains higher concentrations of non-radiogenic Pb, with mean F207% of 4.8%. The lower intercept of the Terra-Wasserburg concordia gives an age of 1046.8 \pm 5.6 Ma (MSWD = 1), which is within error of the published U-Pb age for BLR-1 titanite (1047.10 \pm 0.40 Ma, Aleinikoff et al., 2007; Spencer et al., 2013, Stearns et al., 2016). The $^{207}\text{Pb-corrected}$ $^{206}\text{Pb}/^{238}\text{U}$ ratios for this sample yielded ages with a weighted mean average of 1046.5 \pm 3.2 Ma (MSWD = 1.2, Table 4).

Table 2
Summary of EMP analyses.

BLR-1 $(n = 19)$		BLR-2 ($n = 55$)		Ecstall (n = 26)		McClure (n = 22)		BRA-1 $(n = 71)$		FCT (n = 26)		
Elements	Concentration (ppm) ¹	RSD (%) ²	Concentration (ppm)	RSD (%)	Concentration (ppm)	RSD (%)	Concentration (ppm)	RSD (%)	Concentration (ppm)	RSD (%)	Concentration (ppm)	RSD (%)
Na	2368	7.1	2486	6.9	182	37.1	346	27.1	139	66.3	242	39.7
F	7971	18.6	6076	21.9	1883	53.3	2338	45.3	1960	54.8	2215	57.3
Al	7253	2.4	6846	4.1	5500	10.4	8664	7.6	8277	7.6	7018	5.9
Si	139815	0.6	139512	2.3	138423	0.9	136041	1.5	142624	1.6	135032	1.4
Ti	213261	1.0	212448	0.6	229787	0.8	223565	1.0	229653	1.1	217928	1.5
K	26	112.1	17	153.3	29	82.3	26	102.5	20	116.7	34	114.6
Ca	198227	0.4	196686	0.3	200786	0.8	202734	0.6	205679	0.3	189394	1.5
Cr	135	34.3	135	33.9	71	57.2	20	113.7	45	65.0	6	218.8
Fe	17091	1.8	16694	2.6	8510	10.9	5897	7.4	5435	8.6	15297	11.5
Mn	671	17.3	676	16.4	928	14.7	333	35.9	654	19.8	2055	16.8
Zr	1496	9.4	1468	5.2	366	38.9	3026	9.7	3	420.6	644	15.5
Sr	451	14.5	436	12.8	161	32.2	497	6.9	159	31.9	127	39.8
Nb	4888	7.5	5146	12.6	884	31.7	2369	27.1	274	81.5	1548	10.6
Ce	2336	4.4	2106	6.0	5291	26.8	3966	9.7	493	16.9	12323	5.8
Nd	1385	7.9	1273	9.2	2100	20.9	1676	11.6	37	128.0	6891	19.3
Mg	461	5.7	419	6.9	48	37.7	62	37.9	13	78.9	177	22.8
Y	652	9.3	565	11.2	1096	24.8	596	12.7	237	43.3	4369	37.0
Th	309	14.5	242	21.8	687	36.8	143	26.0	14	145.9	273	17.4
U	74	72.3	49	104.6	157	69.9	13	265.2	1	513.3	10	202.1
O	397214	0.4	395251	0.8	401319	0.5	398268	0.7	407527	0.5	391872	0.7
Total	996083	0.5	988530	0.6	998206	0.4	990579	0.7	1003245	0.4	987456	0.5
Oxide	770003	0.5	700330	0.0	JJ0200	0.4	JJ037 J	0.7	1003243	0.4	707 430	0.5
Na ₂ O	3192	7.1	3351	6.9	245	37.1	467	27.1	187	66.3	326	39.7
F	7971	18.6	6076	21.9	1883	53.3	2338	45.3	1960	54.8	2215	57.3
Al_2O_3	13705	2.4	12935	4.1	10391	10.4	16371	7.6	15639	7.6	13260	5.9
SiO ₂	299117	0.6	298469	2.3	296137	0.9	291042	1.5	305127	1.6	288885	1.4
TiO_2	355731	1.0	354375	0.6	383297	0.9	372918	1.0	383075	1.0	363515	1.5
K ₂ O	32	112.1	20	153.3	35	82.3	31	102.5	24	116.7	41	114.6
CaO	32 277359	0.4	275203	0.3	280940	0.8	283666	0.6	287786	0.3	265000	1.5
	197	34.3	198	33.9	104	57.2	283000	113.7	66	65.0	203000	218.7
Cr ₂ O ₃ FeO	21988	1.8			10948		7587	7.4	6992			
MnO			21477	2.6		10.9		7.4 35.9		8.6	19679	11.5
	866	17.3	873	16.4	1199	14.7	429		845	19.8	2653	16.8
ZrO ₂	2021	9.4	1983	5.2	495	38.9	4087	9.7	5	420.2	871	15.5
SrO	534	14.5	516	12.8	190	32.2	588	6.9	188	31.9	151	39.8
Nb ₂ O ₅	6993	7.5	7362	12.6	1264	31.7	3389	27.1	393	81.5	2214	10.6
Ce ₂ O ₃	2736	4.4	2467	6.0	6197	26.8	4646	9.7	578	16.9	14434	5.8
Nd ₂ O ₃	1615	7.9	1485	9.2	2449	20.9	1955	11.6	43	128.0	8038	19.3
MgO	765	5.7	695	6.9	80	37.7	103	37.9	21	78.9	293	22.8
Y_2O_3	828	9.3	718	11.2	1391	24.8	757	12.7	301	43.3	5548	37.0
ThO_2	351	14.5	275	21.8	782	36.8	162	26.0	16	145.9	311	17.4
UO_2	84	72.3	55	104.7	178	69.9	14	265.2	1	515.0	12	202.2
Total	996083	0.5	988530	0.6	998206	0.4	990579	0.7	1003245	0.4	987456	0.5

 $^{^{1}}$ Concentrations are mean values of individual spot analyses; The number of spot analyses is marked in brackets, next to the sample's name; 2 RSD = Relative Standard Deviation (RSD = (SD/Mean)*100).

Twenty-four analyses on the Ecstall titanite define a linear array on a Tera-Wasserburg diagram with a lower intercept of 89.6 \pm 2.3 Ma (MSWD = 0.8) and upper intercept ($^{207}\text{Pb}/^{206}\text{Pb})_o$ of 0.740 \pm 0.110. Ecstall titanite has a relatively small amount of non-radiogenic Pb, yielding a mean F207% value of 13%. The weighted mean average of the individual $^{207}\text{Pb}\text{-corrected}$ ages is 90.2 \pm 0.7 Ma (MSWD = 0.6), which is within error of the zircon U-Pb age for the Ecstall pluton (91.50 \pm 1.00 Ma; Butler et al., 2002).

Thirty spot analyses on the BRA-1 titanite define a linear array on a Tera-Wasserburg diagram with a lower intercept of 519.3 \pm 23 Ma (MSWD = 0.8) and a $^{207}\text{Pb}/^{206}\text{Pb}$ value of 0.864 \pm 0.032 at the ordinate. These data reflect varying abundances of radiogenic and non-radiogenic Pb components. At the lower end of the discordia array (closer to the x-axis), spot analyses reflect \sim 25% non-radiogenic Pb, whereas towards the upper intercept (closer to the y-axis), the main cluster of spot analyses indicates up to ca. 60% non-radiogenic Pb content (Fig. 3 and Table 4). The weighted mean age calculated from the individual $^{207}\text{Pb-corrected}$ ages for the BRA-1 sample is 532.7 \pm 9.9 Ma (MSWD = 0.7).

The U-Pb spot analyses on the McClure titanite (n=39) form a cluster on and slightly off concordia (Fig. 3) with low amounts of non-radiogenic Pb (F207% values ranging from 0.05% to 1.7%). Three spot analyses yielded negative F207% values. There are several

explanations for negative F207% values: the non-radiogenic Pb concentrations may have been below limits of detection (Table S2), the composition of the non-radiogenic component is inaccurate, or the sample experienced $^{207} {\rm Pb}/^{206} {\rm Pb}$ fractionation. The uncorrected isotopic ratios of all analyses yield concordia age of 524.8 \pm 2.3 Ma (MSWD = 4.6), and a $^{206} {\rm Pb}/^{238} {\rm U}$ weighted mean age of 520.3 \pm 2.4 Ma (MSWD = 1.2). Both the isochron and the weighted mean ages overlap within uncertainty of the published titanite U-Pb ID-TIMS age (523.26 \pm 1.27 Ma, Schoene and Bowring, 2006).

A total of 25 spot analyses on the FCT titanite define a statistically significant linear array on a Tera-Wasserburg diagram with a lower concordia intercept of 28.3 ± 3.9 Ma (MSWD =1.2) and an upper $^{207}\text{Pb/}^{206}\text{Pb}$ ratio of $0.886\pm0.082.$ The FCT titanite yielded a high F207% value, with a mean of 56.4%, the spread in the data between concordia (no non-radiogenic Pb) and the upper intercept which provides a good control in determining a robust crystallization age and the isotopic composition of the initial Pb component. The weighted mean age calculated from $^{207}\text{Pb-corrected}$ data is 29.5 ± 0.8 Ma, with an MSWD of 1.2. For the FCT titanite, both the intercept age and the $^{207}\text{Pb-corrected}$ age are within uncertainty of the published titanite U-Pb ID-TIMS age (28.87 \pm 0.50 Ma; Schmitz and Bowring, 2001).

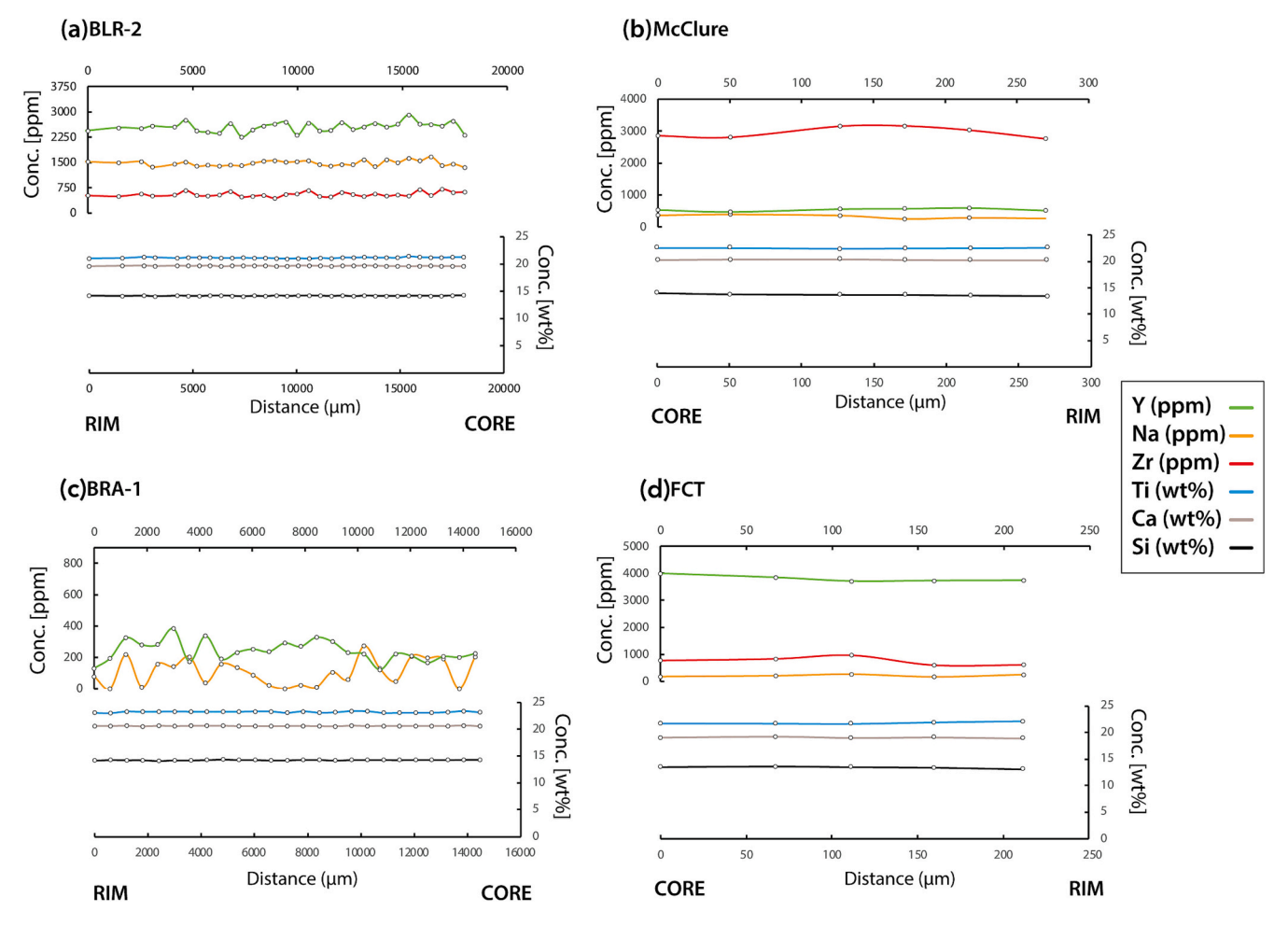


Fig. 2. Chemical transects from core to rim in titanite grains (a) BLR-2, (b) McClure, (c) BRA-1 and (d) Fish Canyon titanite using electron microprobe analyses to determine homogeneity in minor and major elements.

3.3.3. Trace element concentrations using matrix matched and non-matrix matched standard reference materials

In the following two sections, we investigate the effect of using a matrix matched (BLR-1) and a non-matrix matched standard (NIST612 glass) as the primary reference material to calculate titanite trace element concentrations and to correct for instrumental drift. In both cases, we investigated the effect of using Ca, Si or Ti as the internal elemental standard (IES). In order to test the ability of Ca, Si and Ti to serve as an IES, we calculated the trace element fractionation index in BLR-1 and NIST612, relative to these three elements (Fryer et al., 1995). The Elemental Fractionation Index (EFI) was calculated following background correction by dividing the intensity of each element ratioed to the intensity of the IES for the second half (\sim 20 s) of the total integration time by the same intensity ratio for the first half of the integration time. The corresponding fractionation indices are presented in Supplementary Materials Table S3 and Fig. S2. Our results revealed no significant elemental fractionation (IES \sim 1) relative to Ca (IES: 0.99-1.08), Si (0.91-1.00) and Ti (0.97-1.06) for BLR-1 titanite, Similarly, no significant time dependent elemental fractionation was observed for the NIST612 glass relative to Ca (IES: 0.92-1.01) and Si (IES: 0.88-0.97). However, severe elemental fractionation was found in NIST612 relative to Ti (IES \sim 3). This could be attributed to the relatively low Ti concentration in the NIST612 synthetic glass (44 ppm; preferred value from GEOREM) compared to natural titanite (typically 18.16 wt%). Overall, our EFI results for BRL-1 titanite and NIST612 glass demonstrate the suitability of using Ca, Si and Ti as the normalizing elements during the matrix-matched reduction. Similarly, Ca and Si are suited to serve are IES during the non-matrix-matched reduction.

However, due to the severe time-dependent fractionation of Ti in NIST612 glass, its use as the IES for trace element quantification can compromise the results. Importantly, the EFI is dependent not only on the matrix, but also on the laser ablation conditions, therefore these results are only pertinent for the specific parameters employed in this study (See Table 1). In addition to the internal standardization, we also performed a "semi-quantitative" standardization approach (SQ), using BLR-1 as the primary reference material. The SQ standardization in Iolite v. 3 refers to a direct normalization of unknowns relative to the drift-corrected reference material without IES standardization. In presenting the results in the next section, we will refer to Y, Zr, La concentrations and chondrite-normalized REE topography proxies. The detailed results for all standardization approaches tested can be found in Supplementary materials Table S3. All uncertainties reported in this section are 2 standard error of the mean (2SE).

The BRA-1 titanite data reduction using BLR-1 as the primary reference material yielded similar Y values for all IES as follows: mean Y values of 53.84 ± 1.33 ppm (Ca IES), 52.76 ± 1.24 ppm (Si IES), 47.79 ± 1.03 ppm (Ti IES).The semi-quantitative DRS yields mean Y concentrations of 49.42 ± 3.13 ppm (SQ). The Zr concentrations do not seem to vary significantly with the IES used, nor do they vary between the reduction methods (internal standardization vs. semi-quantitative), with the four approaches yielding mean values of 29.34 ± 1.12 ppm (Ca IES), 29.69 ± 1.19 ppm (Si IES), 27.03 ± 1.03 ppm (Ti IES), and 27.11 ± 2.19 ppm (SQ). The La concentrations yield a mean value of 0.10 ± 0.01 ppm for all three IES (Ca, Si and Ti), whereas the semi-quantitative approach gives a slightly higher mean value of 0.19 ± 0.02 ppm (SQ). The REE trends for the BRA-1 sample show strong depletion in LREE

Table 3
Solution ICPMS data.

Element	Unit	BLR-2		BRA-1		
		Core	Rim	Core	Rim	
As	ppm	3.87	3.86	1.27	1.21	
Ba	ppm	16.25	19.21	< D.L.	< D.L.	
Ве	ppm	0.23	0.15	< D.L.	< D.L.	
Bi	ppm	0.77	0.77	0.48	0.21	
Cd	ppm	0.82	0.85	0.25	0.22	
Co	ppm	1.70	0.40	0.36	0.40	
Cr	ppm	117.36	100.98	4.01	5.63	
Cs	ppm	0.04	0.05	< D.L.	< D.L.	
Cu	ppm	6.03	3.83	4.50	5.19	
Ga	ppm	12.23	12.38	2.07	1.88	
Ge	ppm	16.60	16.78	5.75	5.65	
Hf	ppm	33.84	37.20	4.26	4.78	
In	ppm	< D.L.	< D.L.	< D.L.	< D.L.	
Mo	ppm	5.89	5.68	10.75	11.55	
Nb	ppm	7058.77	8008.45	210.07	140.55	
Ni	ppm	716.13	14.23	27.53	37.90	
Pb	ppm	37.74	59.11	3.00	6.27	
Rb	ppm	0.75	0.96	< D.L.	< D.L.	
Sb	ppm	1.30	1.15	0.19	0.49	
Sn	ppm	67.83	125.28	12.69	13.29	
Sr	ppm	306.96	317.41	29.02	22.27	
Ta	ppm	417.65	606.11	30.65	15.99	
Th	ppm	238.71	225.20	0.10	0.22	
U	ppm	110.15	100.53	2.68	0.97	
V	ppm	266.32	270.01	345.48	342.79	
W	ppm	< D.L.	1.21	0.89	0.84	
Y	ppm	614.55	605.59	127.29	48.60	
Zn	ppm	20.15	19.36	12.72	10.50	
Zr	ppm	1578.20	1702.27	34.37	35.81	
La	ppm	402.07	418.41	0.71	0.55	
Ce	ppm	1640.33	1676.40	4.36	2.60	
Pr	ppm	284.90	291.86	1.21	0.60	
Nd	ppm	1223.55	1234.48	8.51	3.48	
Sm	ppm	278.88	280.00	5.51	1.94	
Eu	ppm	64.01	63.93	2.50	0.84	
Gd	ppm	183.03	183.18	9.00	2.96	
Tb	ppm	27.62	27.46	2.33	0.78	
Dy	ppm	154.79	153.59	19.38	6.72	
Но	ppm	27.44	27.06	4.69	1.73	
Er	ppm	66.80	66.38	14.50	5.94	
Tm	ppm	8.85	8.71	2.48	1.14	
Yb	ppm	49.63	48.91	18.05	9.16	
Lu	ppm	5.27	5.20	2.59	1.38	

Note: < D.L. - below detection limit.

 $([La/Yb]_N \ of \ 0.003 \ for \ IES-reduction \ and \ 0.005 \ with \ SQ-reduction)$ and significant enrichment in HREE with a $[Dy/Yb]_N$ of 0.200, for both IES and SQ reductions. The Eu anomaly calculated using the BLR-1-reduced data are negative (Eu/Eu* =0.740) (for all three IES reductions), with slightly higher values using SQ-reduction (mean of 0.76). Significant differences between the results of IES-reduction and SQ-reduction for the BRA-1 titanite have been observed for Ta, with the SQ techniques

generating concentrations two times higher than the IS method (14.61 \pm 0.92 ppm for SQ and around 7 ppm for IES, Supplementary materials Table S3).

Trace element data for Ecstall titanite, normalized relative to BLR-1 as the primary standard, yield high Y concentrations with mean values of 1321.35 \pm 45.37 ppm (Ca IES), 1315.49 \pm 43.35 ppm (Si IES), 1296.49 ± 41.51 ppm (Ti IES), and are within uncertainty, whereas the SQ approach yields lower Y concentrations of 1185.24 \pm 77.82 ppm. Values of La are also high and within uncertainty for the IES reductions, with means of 1701.17 \pm 52.06 ppm (Ca IES), 1707.36 \pm 55.72 ppm (Si IES) and 1666.83 \pm 51.70 ppm (Ti IES). Lanthanum values obtained via the SQ reduction are outside uncertainty, with a lower mean of 1503.18 \pm 92.06 ppm. The Zr mean concentrations for Ecstall titanite are 409.16 \pm 11.63 ppm (Ca IES), 405.81 \pm 10.22 ppm (Si IES), and 400.97 \pm 9.33 ppm (Ti IES), whereas the SQ reduction generated lower values with a mean of 366.37 \pm 22.98 ppm. The REE trends for Ecstall samples show enrichment in LREE with [La/Yb]_N values around 8, a very small negative Eu anomaly of 0.750 and slight depletion in HREE ([Dy/Yb]_N of 1.220; Fig. 4, Supplementary materials Table S3). The main difference between the reduction techniques is reflected in the LREE to HREE ratio, as the Si-reduction gives a lower value of 6.970 for [La/Yb]_N, compared to 8.420 (Ca IES), 8.780 (Ti IES) and 9.280 (SQ).

McClure titanite yielded mean Y values within uncertainty for all reduction techniques relative to BLR-1 titanite: 626.76 ± 15.91 ppm (Ca IES), 596.60 \pm 15.34 ppm (Si IES), and 604.45 \pm 13.68 ppm (Ti IES). Moreover, comparable concentrations are obtained when the SQ reduction is used (589.92 \pm 35.73 ppm). Similar to Ecstall, the McClure sample has high Zr concentrations, yielding means of 2673.24 \pm 65.12 ppm (Ca IES), 2548.94 \pm 70.55 ppm (Si IES), 2586.47 \pm 57.16 ppm (Ti IES), and 2522.86 \pm 171.84 ppm (SQ). Furthermore, La values are also high, yielding means of 1158 \pm 28 ppm (Ca IES), 1107 \pm 30 ppm (Si IES), 1117 \pm 26 ppm (Ti IES), and 1118 \pm 76 ppm (SQ). The REE spider diagrams for McClure titanite display enrichment in LREE with [La/ Yb]_N ratios of \sim 16, a slight depletion in HREE, with [Dy/Yb]_N of 1.7, and a small positive Eu anomaly (Eu/Eu* = 1.3; Supplementary Materials Table S3). No significant differences were observed between the results of the various reduction approaches using BLR-1 titanite, in terms of rare earth elements.

The matrix-matched reduction of FCT titanite yielded high Y values: 30001.00 ± 832.00 ppm (Ca IES), 28198.40 ± 818.00 ppm (Si IES), 32097.60 ± 750.00 ppm (Ti IES) and 27697.20 ± 1598.80 ppm (SQ). FCT Zr concentrations are also high, with mean values of 673.24 ± 19.32 ppm (Ca IES), 630.56 ± 17.92 ppm (Si IES), 717.87 ± 17.40 ppm (Ti IES) and 608.16 ± 34.44 ppm (SQ). Additionally, mean La concentrations range from 2685.20 ± 152.40 ppm (SQ) to 3101.12 ± 65.68 ppm (Ti IES). For the REE composition, FCT shows a fairly flat trend ([La/Yb] $_N$ = 0.730), a slight HREE depletion ([Dy/Yb] $_N$ = 1.230), and a well-marked negative Eu anomaly (Eu/Eu* = 0.190; Supplementary Materials Table S3). Overall, the REE trends are independent of the reduction protocol when BLR-1 is used as the primary standard.

Table 4 Summary of titanite ages.

Sample	Intercept ages and errors		Intercept ages and errors		Intercept ages and errors		Intercept ages and errors $(^{207}\text{Pb}/^{206}\text{Pb})_0$		How is $(^{207}Pb/^{206}Pb)_0$ constrained?	Pb _{cm} -corrected ages a	Pb _{cm} -corrected ages and errors		
	Intercept age (Ma)	2σ	MSWD			Weighted age (Ma)	2σ	MSWD					
BLR-2	1046.8	5.6	1.0	1.000 ± 0.140	2D isochron	1046.5	3.2	1.2	$1047.10 \pm 0.40 \ \text{Ma}^{1}$				
Ecstall	89.6	2.3	0.8	0.740 ± 0.110	2D isochron	90.2	0.7	0.6	$91.50 \pm 1.00 \text{ Ma}^2$				
McClure	524.8*	2.3	4.6	_	_	520.3*	2.4	1.2	$523.26 \pm 1.27 \text{ Ma}^3$				
BRA-1	519.3	23.0	0.8	0.864 ± 0.032	2D isochron	532.7	9.9	0.7	_				
FCT	28.3	3.9	1.2	0.886 ± 0.082	2D isochron	29.5	0.8	1.2	$28.87 \pm 0.50 \; \text{Ma}^{\text{4}}$				

Ages are quoted with 95% confidence interval.

- * Concordia age; The ²⁰⁶Pb/²³⁸U weighted mean age is uncorrected for Pb_{cm}.
- ¹ Published age for BLR-1 titanite; Aleinikoff et al., 2007
- ² Zircon U—Pb age; Butler et al., 2002
- 3 (207 Pb/ 235 U) age of 523.26 \pm 1.27 Ma; Schoene and Bowring, 2006

⁴ Schmitz and Bowring, 2001

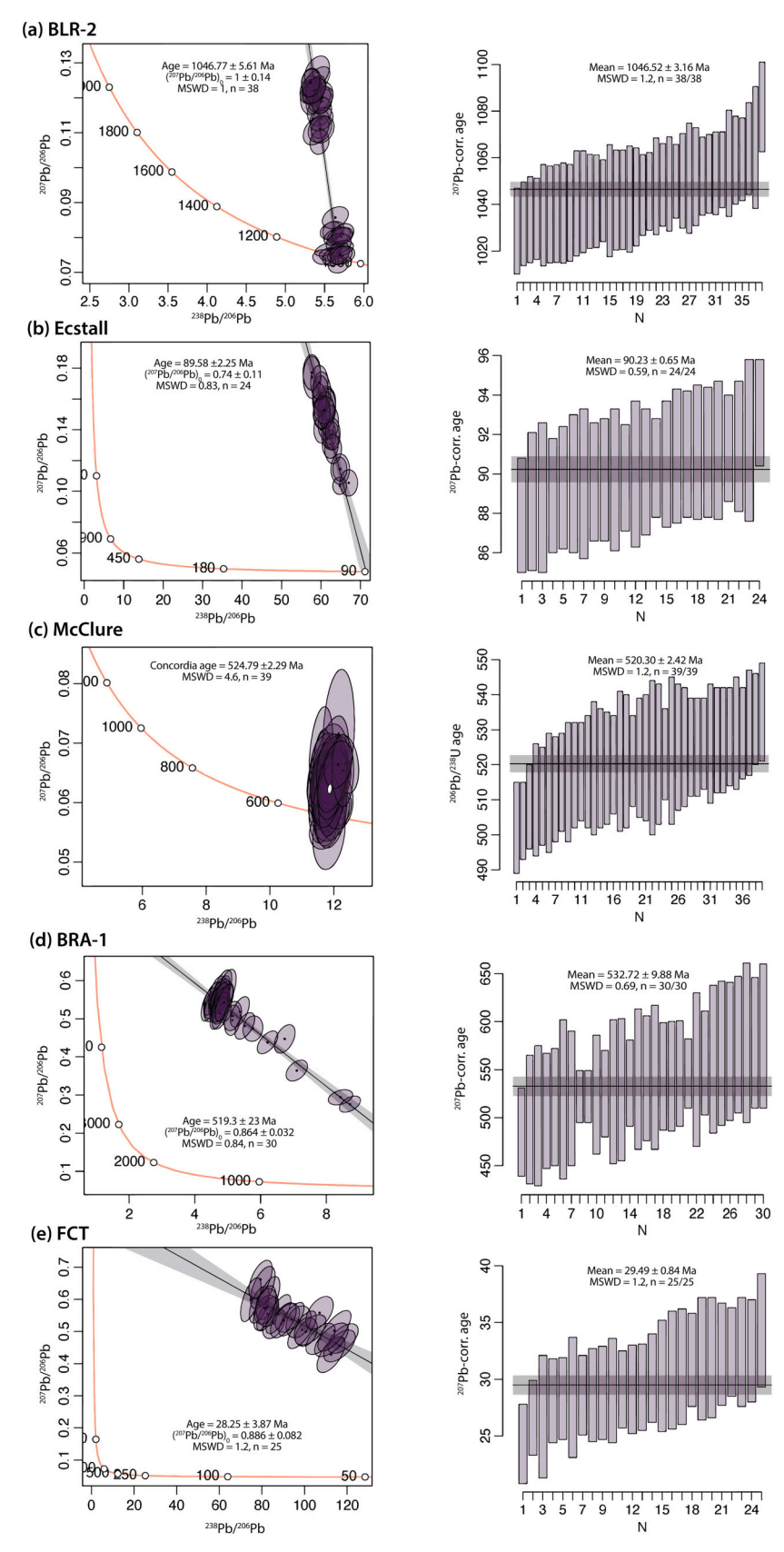


Fig. 3. U—Pb data and calculated ages for new and existing titanite reference materials: (a) BLR-2, (b) Ecstall, (c) McClure, (d) BRA-1 and (e) Fish Canyon titanite. On the left: Tera-Wasserburg diagrams of uncorrected U—Pb data and on the right: ²⁰⁷Pb-corrected weighted U—Pb ages. For sample McClure: on the right: the uncorrected ²⁰⁶Pb/²³⁸U weighted mean age. Plots made using IsoplotR (Vermeesch, 2018).

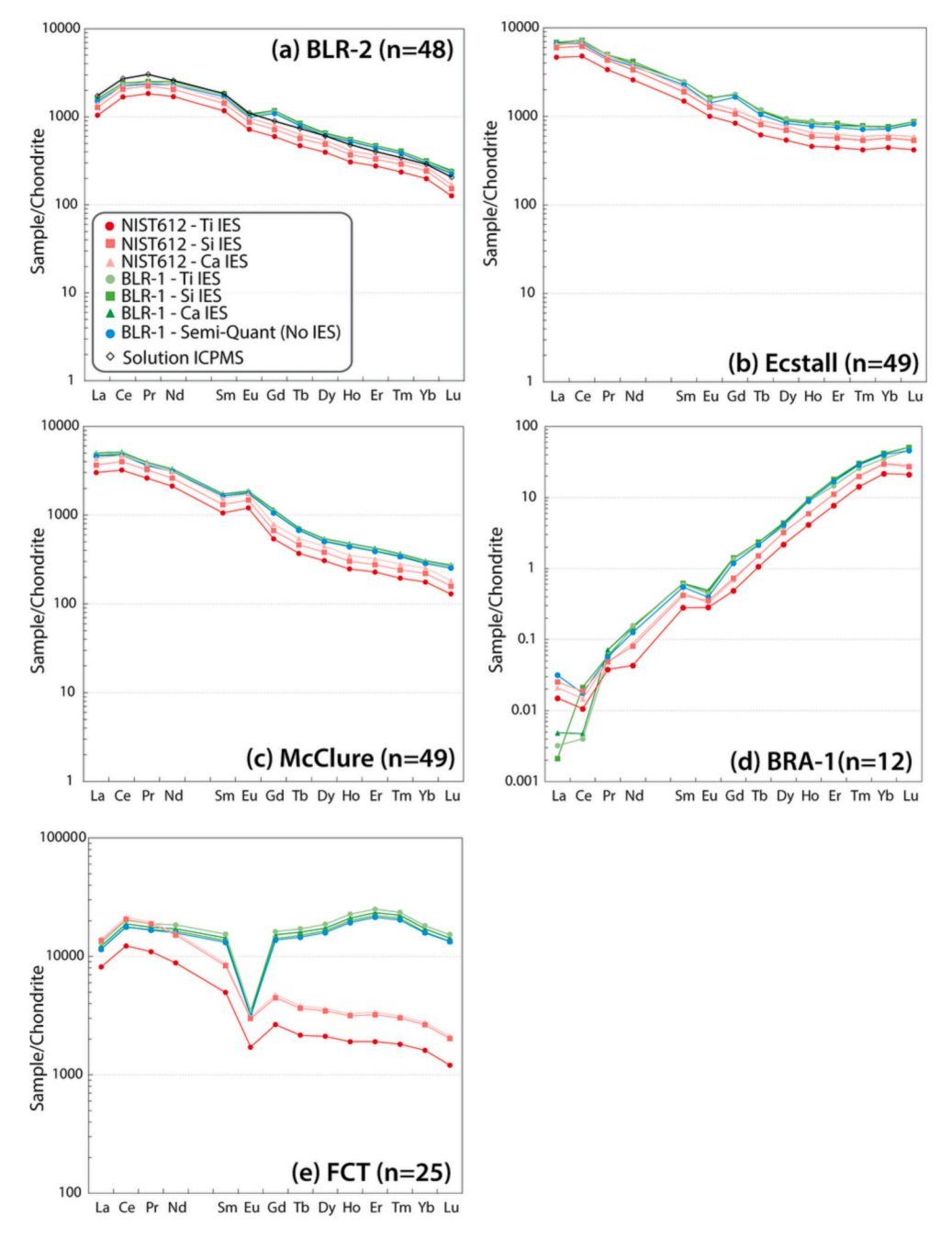


Fig. 4. Chondrite-normalized REE spider diagrams for each grain and each DRS approach. Chondrite REE values are from Barrat et al. (2012). Each line represents the median value of individual spot analyses.

Matrix-matched data reduction for BLR-2 titanite yielded mean Y concentrations of 623.51 \pm 14.46 ppm (Ca IES), 614.60 \pm 12.14 ppm (Si IES), 586.00 \pm 11.28 ppm (Ti IES), and 588.42 \pm 37.98 ppm (SQ). High Zr concentrations for BRL-2 titanite were obtained for all four reduction approaches with means of 1674.77 \pm 41.44 ppm (Ca IES), 1663.17 \pm 32.94 ppm (Si IES), 1564.02 \pm 31.75 ppm (Ti IES), and a mean of 1576.88 \pm 99.17 ppm (SQ). Mean La values obtained using the IS method range from 345.30 \pm 5.98 ppm (Ti IES) to 364.60 \pm 7.42 ppm (Si IES). Whereas the SQ approach yielded 366.15 \pm 25.27 ppm La. For the REE trends, BLR-2 titanite shows enrichment in LREE with mean [La/Yb]_N values of 4.700 when the internal standardization method is used and higher [La/Yb]_N values from the semi-quantitative approach, with a mean of 5.060. The matrix-matched reduction generated [Dy/Yb]_N mean values of 2.100. These ratios indicate a moderate depletion

in HREE for the BLR-2 titanite. Europium anomalies are independent of the reduction protocol when BLR-1 is used as the primary standard, with a mean value of 0.7.

Mean Y values obtained for BRA-1 titanite using NIST612 as the primary standard are 43.50 \pm 1.05 ppm (Ca IES), 40.93 \pm 10.90 ppm (Si IES) and 25.89 \pm 0.52 ppm (Ti IES). The Zr concentration depends on the IES employed, with mean values of 27.40 \pm 1.04 ppm (Ca IES) and 25.56 \pm 1.00 (Si IES), and a mean of 16.84 \pm 0.71 ppm (Ti IES). Similarly, La concentration consistently varies with the elemental standard used, Ca and Si approaches yielding mean values of 0.17 \pm 0.02 ppm, whereas Ti yields a mean Zr concentration of 0.10 \pm 0.01 ppm. For the REE trends, some of the relevant normalized ratios for the BRA-1 sample are [La/Yb]_N = 0.005, [Dy/Yb]_N of 0.200 and Eu/Eu* of 0.860, and these ratios do not vary significantly with the IES used (Supplementary Materials Table S3).

The mean Y, Zr and La concentrations determined using NIST612 glass for Ecstall titanite are smaller than the values obtained via BLR-1 reduction. With Y yielding concentrations of 1068.56 ± 35.10 ppm (Ca IES), 946.13 ± 29.69 ppm (Si IES) and 741.46 ± 22.63 ppm (Ti IES). Whereas Zr yielded concentrations of 395.94 ± 10.44 ppm (Ca IES), 352.28 ± 9.33 ppm (Si IES) and 267.28 ± 6.22 ppm (Ti IES). Finally, La yielded concentrations of 1451.46 ± 40.23 ppm (Ca IES), 1304.60 ± 34.23 ppm (Si IES) and only 1002.20 ± 25.41 ppm (Ti IES). The REE trends do not vary significantly from the values obtained relative to BLR-1, although NIST612-reduction yielded a less pronounced negative Eu anomaly (Eu/Eu* =0.900 versus 0.750).

The Y concentrations for McClure titanite are lower using NIST612 glass (compared to BLR-1 standardization), with mean values of 505.50 \pm 12.76 ppm (Ca IES), 438.20 \pm 11.18 ppm (Si IES) and 349.92 \pm 7.97 ppm (Ti IES). Correspondingly, the Zr and La abundances are also smaller when NIST612 glass is used. For Zr, mean concentrations of 2581.39 \pm 62.39 ppm (Ca IES), 2225.43 \pm 61.33 ppm (Si IES), and 1738.27 \pm 38.24 ppm (Ti IES). Whereas La yielded median concentrations of 1023.86 \pm 24.51 ppm (Ca IES), 891.45 \pm 23.49 ppm (Si IES), and 704.10 \pm 15.87 ppm (Ti IES). Somewhat higher values are obtained for the REE ratios: Eu/Eu* = 1.610, [Dy/Yb]_N = 1.710 and [La/Yb]_N = 17.000 (Fig. 4).

The trace element reduction for FCT titanite using NIST612 yielded Y mean concentrations of 5763.44 \pm 159.40 ppm (Ca IES), 5485.28 \pm 159.44 ppm (Si IES), and only 3255.12 \pm 75.76 ppm (Ti IES). Whereas La yielded mean concentrations of 3345.56 \pm 77.52 ppm (Ca IES), 3203.28 \pm 70.32 ppm (Si IES), and 1928.56 \pm 40.76 ppm (Ti IES). Finally, Zr yielded mean concentrations of 722.36 \pm 20.68 ppm (Ca IES), 690.52 \pm 19.56 ppm (Si IES), and 399.36 \pm 9.62 ppm (Ti IES). The Eu anomalies are negative (Eu/Eu* = 0.4). The [La/Yb]_N yields a slight enrichment in LREE ([La/Yb]_N = 5.2), whereas the [Dy/Yb]_N = 1.6, yields a relatively flat HREE pattern (Fig. 4).

The BLR-2 titanite yielded Y values of 499.74 \pm 11.65 ppm (Ca IES), 452.91 \pm 8.81 ppm (Si IES), and 360.62 \pm 6.96 ppm (Ti IES), high Zr concentrations of 1606.10 \pm 40.17 ppm (Ca IES), 1445.44 \pm 28.31 ppm (Si IES), and 1126.05 \pm 23.28 ppm (Ti IES). The La concentrations yield means of 329.52 \pm 6.60 ppm (Ca IES), 300.03 \pm 5.91 ppm, and 236.15 \pm 4.08 ppm, respectively. The REE results from the non-matrix-matched reduction for BLR-2 titanite are similar in the overall trends to the BLR-1 reduction output data, with significant fractionation between the light and the heavy REE ([La/Yb]_N 5.230), a moderate enrichment in HREE ([Dy/Yb]_N = 2.010) and a small, negative Eu anomaly (Eu/Eu* = 0.860)), regardless of the IES used (Fig. 4).

4. Discussion

4.1. Which titanite reference material can be used for trace element standardization?

The chemical characterization of the analyzed titanite grains (BLR-2, Ecstall, BRA-1, McClure and FCT) serves to determine their suitability to be used as standard reference materials for titanite petrochronology via LA-ICPMS. Our study shows that BLR-1 can be used as a primary standard to precisely and accurately determine trace element concentrations and U-Pb ratios. The BLR-1 titanite is extensively used in titanite U-Pb dating as a primary reference material (e.g., Stearns et al., 2016), or a secondary age standard (e.g., Kirkland et al., 2017) because of its isotopic homogeneity and its ability to provide a reliable matrix-matched down-hole correction. The chemical homogeneity in major and trace elements of the BLR-1 titanite highlighted in this study by the narrow range of chemical concentrations. The RSD (%) for major elements is <1% for Ti, Si, and Ca, whereas most of the other elements have RSD <10% (Fig. 2 and Table S3). The BLR-1 trace element values attained by normalizing to NIST612 glass also support its homogeneity (Supplementary Materials Table S3).

The BLR-2 titanite grain proved to be chemically homogeneous, as shown by the EMP (Table 2) and LA-ICPMS (Table S3) data and suitable to serve as a primary reference material for titanite trace element analysis. In contrast, the heterogeneity displayed by Ecstall, McClure and FCT titanite grains, makes these grains unsuitable to serve as reference materials for trace element quantification. Similarly, the BRA-1 titanite shows high intra-sample chemical heterogeneity with total REE concentrations of 96 ppm (core) and 40 ppm (rim) while also having low trace elemental abundances. Therefore, we recommend that it is not used in any capacity in the titanite LA-ICPMS trace elements data standardization.

4.2. The influence of using matrix-matched RMs and IES for trace element characterization

It is commonly asserted that using a matrix-matched reference material reduces the effect of the laser-induced elemental fractionation during ablation by providing a robust downhole fractionation correction. However, there have been few attempts to quantify the differences between standardization with a matrix-matched and a non-matrix-matched reference material.

A comparative time-resolved investigation of the CPS for BLR-1 titanite, NIST612 glass and Ecstall, McClure and FCT titanites shows that the matrix-matched reference material (BLR-1) displays a similar CPS-time(s) slope to the titanite samples when compared to the NIST612 glass (Fig. 5, Table S3). The slope consistency among titanite reference materials suggests that laser-induced downhole fractionation is matrix dependent. We find that the non-matrix-matched reference material NIST612 shows a lower slope across all five elements analyzed. The systematically lower slope yielded by NIST612 may lead to inaccuracies when correcting for downhole fractionation. Therefore, a matrixmatched standardization for titanite trace element determination has the potential to provide a more robust downhole fractionation correction. We quantified the influence of the matrix-matching calibration for trace elements by comparing solution ICPMS concentrations with in-situ LA-HR-ICPMS results (detailed single-spot data can be found in Table S3 and Fig. 6). Our comparison revealed some differences in the results between using the matrix-matched primary standard (BLR-1 titanite) and NIST612 glass. We estimate the percentage of difference (PoD in %) between the reduction results (for BLR-2) and the expected values (solution ICPMS data, Table S3). To determine if differences between corrections are statistically significant, we also applied a two-sample twotailed t-test. This assessment was performed on an element-by-element and DRS-by-DRS basis, and the results are presented in Table S3. The null hypothesis is that the means of the two samples compared at each time are equal and the significance level is 0.05 (Table S3). Furthermore, we applied an additional one-sample two-tailed t-test statistic to evaluate systematic offset between our LA-HR-ICPMS data relative to the solution ICPMS data. The null hypothesis is that there are no systematic offsets between LA-HR-ICPMS trace elemental values and the reference values (i.e., solution ICPMS concentrations), and the significance level is 0.05 (Table S3).

The results of the two-sample *t*-test statistic revealed statistically significant differences between the matrix-matched and the non-matrix-matched reductions for almost all elements, with few exceptions. The semi-quantitative matrix-matched reduction and the non-matrix-matched reduction with Ca as the IES yielded statistically similar elemental concentrations for Nb, Pr and Zr, according to the two-sample *t*-test. Furthermore, for the matrix-matched standardization there is not sufficient evidence to prove that the sample means of the elemental concentrations yielded by Ca and Si as the IES are different. Therefore, we failed to reject the null hypothesis for all elements investigated here (Table S3). Statistically relevant differences have been identified between the use of Ca and Ti and Si and Ti standardizations for Nb, Y, Zr, Sr, MREE and HREE. The internal elemental standard has a more

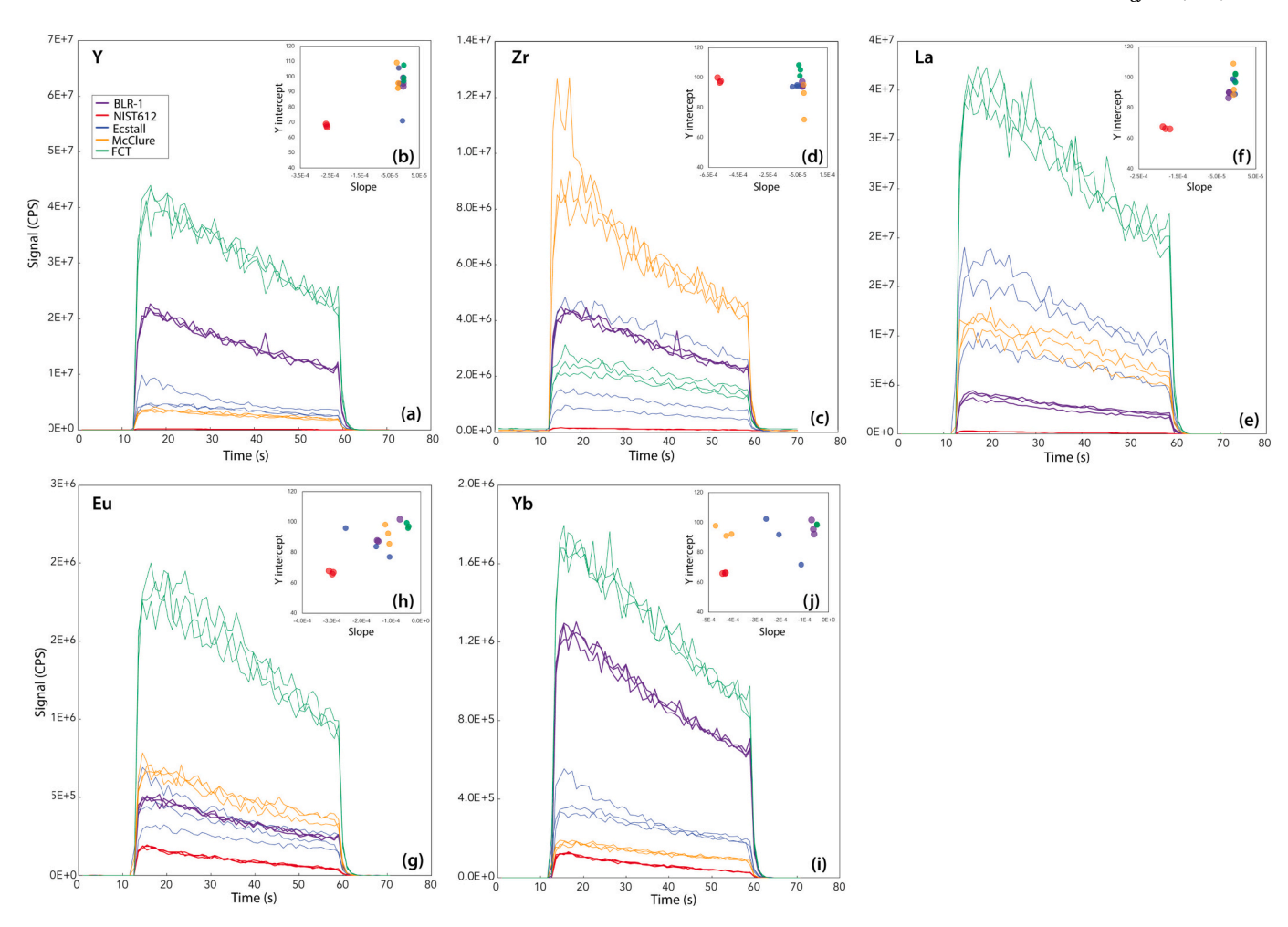


Fig. 5. Y (a), Zr (c), La (e), Eu (g) and Yb (i) downhole counts for 3 analyses on reference materials (BLR-1 and NIST612) and titanite samples (Ecstall, McClure and FCT). Inset plots (b, d, f, h, and j) display calculated slopes of the downhole signal versus Y intercepts for the samples and reference materials for Y, Zr, La, Eu and Yb, respectively.

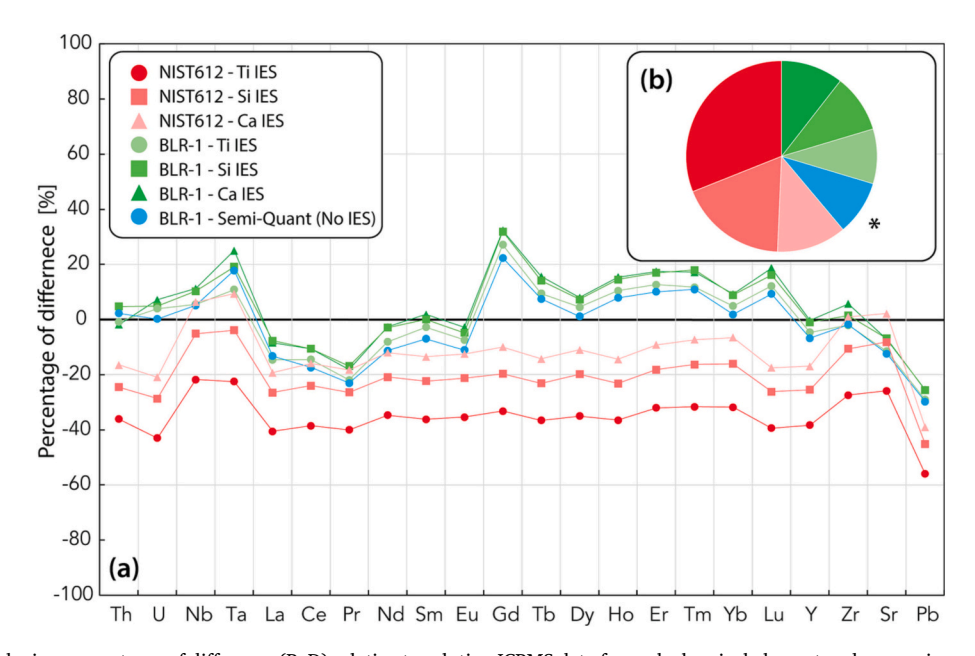


Fig. 6. (a) Line plot displaying percentages of difference (PoD) relative to solution ICPMS data for each chemical element and comparing each standardization mode (matrix-matched vs. non-matrix matched reference materials) and data reduction schemes (internal element standard vs semi-quantitative approach). (b) Pie chart of the weighted PoD for each standardization method.

pronounced effect during non-matrix-matched standardization (NIST612 as the SRM) according to the two-sample t-test, with the null hypothesis being rejected for all elements during all of the reduction combinations investigated (NIST612 – Ca vs NIST612 – Si, NIST612 – Ca vs NIST612 – Ti and NIST612 – Si vs NIST612 – Ti). Consequently, both the SRM and IES employed have statistically significant effects on the resulting trace elemental concentrations.

Our study shows that matrix-matched standardization provides a better reproducibility of elemental abundances for BLR-2 titanite (Fig. 6 and Table S3). The matrix-matched standardizations with Si and Ti as the IES pass the one-sample t-test for the following trace elements via a Si IES: Th, La, Ce, Pr, Nd, Sm, Y, Zr, and Pb and via a Ti IES: Th, U, Ta, Nd, Sm, Yb, Zr, and Pb. These results suggest that the differences observed between the LA-HR-ICPMS trace elemental data and the solution ICPMS reference values are statistically insignificant for these trace elements. In the case of the matrix-matched standardization with Ca as the IES, we fail to reject the null hypothesis for Th, U, La, Nd, Sm, Y and Pb. The semi-quantitative approach generates elemental data with systematic offset relative to the solution ICPMS value for all trace elements except for the Th, U, Dy and Zr concentrations. Whereas for a significant number of the trace elements standardized relative to the BLR-1 titanite the null hypothesis is rejected, our study reveals that the actual difference between our in-situ data and the reference values is generally small (<15% for Th, U, Nb, La, Nd, Sm, Eu, Tb, Dy, Ho, Yb, Y, Zr, Sr and between 15% and 25% for Ta, Pr, Er, Tm, Lu). Although focusing on titanite, we suggest that these findings may have a significant impact on other radiometric techniques such as fission-track and (U-Th-Sm)/He dating in low-U/Th phases such as apatite. As a precise age in these methods is dependent on an accurate estimation of the parent isotope.

The Ce, Nd, Eu, Y, and Pb abundances are closest to the expected values (solution ICPMS data) when Ca is used as the IES during the matrix-matched reduction, with PoD of 10.6%, 2.7%, 2.8%, 0.3%, and 25.5%, respectively. For elements such as La, Pr and Sm, the matrixmatched reduction using Si as the IES generated the best data reproducibility with PoD of 7.6%, 16.8%, and 0.1%, respectively. The matrixmatched standardization relative to Si also best reproduces the HREE topography (PoD for (Dy/Yb)_N of 1.1%). The matrix-matched Tireduction yielded a near-identical Th concentration relative to the solution ICPMS data, differing by only 0.8%. The best reproducibility for U, and most of the HREEs was obtained through the semi-quantitative reduction approach relative to BLR-1 primary standard, with PoD of 0.2% (U), 7.5% (Tb), 1.2% (Dy), 7.9% (Ho), 1.9% (Yb) and 9.3% (Lu). Overall, the major issue of the matrix-matched standardization seems to be that it significantly overestimates Gd concentrations (PoD between 22% and 33%) and Pr (PoD between 16% and 23%) and it systematically generates higher MREEs and HREEs values relative to the solution data. The consistent offset observed here could derive from isobaric mass interferences or that the specific BLR-1 grain used is not representative of published concentrations. The BLR-1 titanite is represented by multiple large crystals that are presumably identical to the grains described by Aleinikoff et al. (2002), Mazdab (2009) and/or Ma et al. (2019). Mazdab (2009) reports a Gd preferred value for BLR-1 titanite of 655 ppm (Instrumental Neutron Activation Analysis, INAA), whereas Ma et al. (2019) report a concentration of 473 ppm (LA-ICPMS). This 32% relative percentage difference between the two values is indicative of a certain inter-grain Gd variability for BLR-1 titanite. As shown in this study by the investigation of the BLR-2 sample, the assumption of trace element homogeneity could lead to inaccurate concentrations if using BLR-1 as a primary reference material. Another explanation for the erroneous measurement of Gd could be LREE mass interference. For titanite with high REE concentrations and enrichment in LREE relative to HREE, a marked CeO isobaric interference on Gd can occur. Moreover, another possible oxide interference on mass 157 (Gd), even if less significant, could come from Pr mass 141. This could also explain the underestimation of Pr concentrations during matrix-match reduction.

NIST612 results are less affected by this due to lower overall trace element concentration. We were unable to correct for these interferences and more work is needed to adequately constrain these masses.

Consequently, few trace elements require reduction relative to a nonmatrix-matched standard (NIST612 glass) for a more accurate concentration determination. For example, Sr abundances obtained relative to Ca differ by only 2.2% from the solution data, when NIST612 is the primary SRM. For elements such as Gd, Er and Tm, the NIST612 reduction with Ca as the IES produces values closest to the solution ICPMS ones, with PoD of 9.9%, 9.1% and 7.3%, respectively. Moreover, the chondrite normalized LREE/HREE ratios, represented by the [La/ $Yb]_N$ value is reproduced best by the Si-reduction relative to the nonmatrix-matched standard (PoD of 15.3%), and the same reduction approach yields an Eu anomaly in good agreement to the solution data, differing by 0.8%. One significant aspect of the NIST612 reduction is that Ti cannot be used as an internal standardization element, possibly due to low Ti concentrations in NIST612 glass with respect to abundance in titanite. Additionally, the non-matrix-matched reduction method underestimates the Pb values by ~50%.

Our study did not reveal a systematic variation among trace element concentrations across the different reduction approaches. However, based on the one sample t-test, two-sample t-test, our element and reduction comparison between LA-HR-ICPMS and solution Q-ICPMS, and the weighted PoD for each standardization method (Fig. 6b.), we suggest that the matrix-matched standardization (relative to BLR-1) yields the most accurate trace element concentrations. More specifically, the matrix-matched reduction using Si as the IES yields the closest match between solution ICP-MS and LA-HR-ICP-MS data, followed by the matrix-matched Ti IES (Fig. 6). Although the matrix-matched semiquantitative standardization approach passes the t-test only for Th, U, Dy and Zr concentrations, it yielded the smallest weighted PoD and yields the best reproducibility in HREE. Therefore, it may be suitable for trace element quantification in situations where a IES characterization of the unknowns via EMP cannot be performed. However, we suggest that this approach needs to be applied with caution and not before confirming the chemical homogeneity of the BLR-1 grain. The semiquantitative procedure is not recommended for reference materials Ecstall, McClure, FCT and BRA-1, due to substantial intra-crystal variation of trace element abundances (see Fig. 2, Table 2, and Table S3).

The use of NIST612 as a primary standard and the internal standardization method relative to Ca or Si are also viable options for trace element quantification, as long as the systematic underestimation of trace elemental values is taken into account. As shown by the data presented in this contribution (see Fig. 6), the NIST612 standardization systematically underestimates the U, Th, Pb, REE + Y concentrations. We suggest that the underestimation is a function of elemental fractionation between titanite and the synthetic glass NIST612 (i.e., the matrix effect) (Fig. 5). Nevertheless, the NIST612 standardization can be used for generating accurate REE ratios (e.g., La/Yb, Sm/Yb) due to the uniform REE underestimation (i.e., flat REE PoD pattern, Fig. 6).

The differences between the results of each reduction scheme can impact titanite petrochronological studies. The temperature-dependent Ti and Zr substitution in titanite make it a useful geothermometer (Hayden et al., 2008). Therefore, accurate determinations of Zr concentrations are paramount for a robust evaluation of thermal evolutions of orogenic and tectonic systems, sensu *lato*. The Zr-in-titanite thermometer is highly sensitive at low- and high-pressure conditions (Hayden et al., 2008). Therefore, we tested the differences in the highest and lowest Zr-in-titanite temperature estimates for all analyzed grains that result from the difference in Zr concentration generated by the different reduction approaches at both low pressure (0.2 GPa) and high pressure (1 GPa) conditions.

In our calculations for FCT titanite we used an SiO_2 activity (a_{SiO2}) of 1 and a TiO_2 activity (a_{TiO2}) of 0.95 (Hayden et al., 2008). For BLR-2, Ecstall, McClure and BRA-1 titanites we have assumed reasonable lower limits for a_{SiO2} and a_{TiO2} of 0.5, typical for crustal rocks (Hayden

and Watson, 2007; Ferry and Watson, 2007). Except for BRA-1, all samples show a temperature difference greater than the uncertainty of the Zr-in-titanite thermometer (\pm 20 °C; Hayden et al., 2008, Table S3). The temperature difference induced by the use of different DRS is minor with maximum temperature difference values for high pressure (1 GPa) calculations of 20.4 °C (BLR-2), 25 °C (Ecstall), 24.9 °C (McClure), 17.1 °C (BRA-1) and 37.6 °C (FCT, Table S3). However, the variation may prove significant for high-resolution, single grain domain studies. These differences will be larger at higher SiO₂ and TiO₂ activity values. Therefore, for high precision Zr-in-titanite temperature calculations, we recommend using the non-matrix-matched standardization (NIST612 as the SRM) with Ca as the IES (PoD of 0.1% relative to solution ICPMS data) or the matrix-matched standardization and Si as the normalizing element, which differs by only 1.5% from the solution ICPMS concentration. The chondrite-normalized HREE topography of titanite can be employed to link titanite growth to the growth of an important petrological mineral, garnet (e.g., Scibiorski et al., 2019). For such studies, the use of the matrix-matched standardization with Si as the normalizing element will provide the most robust [Dy/Yb]_N values. The Th/U ratios and Eu anomalies are effective tools for differentiating between igneous and metamorphic titanites (Olierook et al., 2019). High Th/U ratios and positive Eu anomalies are characteristic of metamorphic titanite. In such studies, the use of the non-matrix-matched standardization (NIST612 as the primary reference material) with Ca as the IES provides the more reliable Th/U and Eu/Eu* values. The NIST612 standardization returns Th/U and Eu/Eu* values with PoD of 0.4% and 0.9%, respectively.

4.3. Reproducible U-Pb age determination in titanite

One of the most frequent approaches to estimate a U-Pb age in titanite is to combine uncorrected U-Pb analyses of a suite of presumed cogenetic titanite grains marked by a large variability in non-radiogenic-Pb. In the best-case scenario, it allows us to define a linear regression on a Tera-Wasserburg diagram and to project an intercept through the ²⁰⁷Pb/²⁰⁶Pb axis determining the initial non-radiogenic Pb composition of the titanite suite. From there, two U-Pb ages can be estimated either by using the lower intercept age or as a weighted average of ²⁰⁷Pbcorrected ages (Simonetti et al., 2006; Chew et al., 2011 for apatite). The spread of the uncorrected U-Pb data and the position of that spread relative to the upper and lower intercepts, a function of the variable incorporation of non-radiogenic Pb quantified by the F207%, is key to calculate precise U-Pb ages (see Kirkland et al., 2017; Kirkland et al., 2018). The F207% can be estimated during an LA-ICP-MS session but it remains unclear how many analyses should be gathered to provide a precise age given the expected uncertainty and the amount of nonradiogenic Pb for each analysis. For titanites with high non-radiogenic Pb concentrations, what is the most suitable spread in Pb_r/Pb_{cm} required for a precise age estimation? Here, we evaluate the effect of variable non-radiogenic Pb content and sample size on the age precision and accuracy using an empirical approach for three titanite RMs which show distinct U-Pb data patterns. Analyses on Ecstall titanite (n = 144) show a moderate range of non-radiogenic Pb content with several analyses being concordant, marking the lower intercept and a low to medium non-radiogenic Pb content (mean F207% of 11.0%, ranging from 0.55 to 48.4%, and a $^{238}\text{U}/^{206}\text{Pb}$ range of 39.9 to 71.3; Fig. 3a). The BRA-1 titanite shows a set of analyses (n = 75) with a large spread of U-Pb data without any concordant analyses at the lower intercept (mean F207% of 54.3%, ranging from 24.6 to 67.0% and a $^{238}\text{U}/^{206}\text{Pb}$ range of 0.03 to 9.07; Fig. 3b). Fish Canyon Tuff titanite U-Pb data (n = 55) shows a moderate spread of high non-radiogenic Pb content (mean F207% of 62.0%, ranging from 42.8 to 83.9% and a $^{238}\text{U}/^{206}\text{Pb}$ ranging from 61.6 to 145.9; Fig. 3c). We applied a bootstrap analysis on each set of titanite analyses with 100 iterations for each subsampling size (i.e., n analyses being 5, 10, 15, 20, 25, 30, 35, 40, 45, 50). We combined this code with the IsoplotR code (Vermeesch, 2018) to calculate a lower intercept age, upper intercept, F207% and weighted mean of ²⁰⁷Pb-corrected age and

their respective uncertainties at each iteration (the R code is available at: https://github.com/antoinetri/titanite_bootstrap). As expected, a larger number of U-Pb analyses increases the chance of obtaining a precise age. The lower intercept ages converge to a narrower age range and the associated uncertainty drops with increasing subsample size by following a power law trend (Fig. 7). The spread in uncertainty significantly decreases after 25 analyses for Ecstall, after 35 analyses for BRA-1 and after 40 analyses for FCT titanite (Fig. 5, Table S4). Similarly, the lower intercept age spread shows a significant decrease after 30 analyses for Ecstall, 35 analyses for BRA-1 and 45 analyses for FCT titanite (Figs. 6 b-d-f). We also calculated the lowest uncertainty obtainable with each titanite U-Pb dataset by extrapolating the power law model, which leads to uncertainties of ± 1.4 Ma (1.6% of relative uncertainty), \pm 29.3 Ma (5.64%) and \pm 4.1 Ma (14.1%) for Ecstall, BRA-1 and FCT titanites, respectively.

After passing the minimum number of analyses mentioned above, the relative uncertainty value is improved, decreasing by ~6.2-6.9% at each step of five analyses (see Table S4 in Supplementary materials). A lower bound exists, after which an increased number of analyses does not improve precision any further (Fig. 7). Our study benchmarks future analytical work in titanite U-Pb dating for which users can reduce their data during a parallel session to estimate the need for additional in situ analyses to reach a given non-radiogenic Pb quantification and U-Pb age uncertainty. For discordant U-Pb data arrays, a minimum of 35 analyses was required to obtain a precise age, depending on the range of nonradiogenic Pb. Obtaining a reliable and precise U-Pb age may not work for some discordant titanite arrays that have a tightly clustered non-radiogenic Pb component in Tera Wasserburg space. In addition to the number of U-Pb analyses, the spread in non-radiogenic Pb content (estimated here by the relative standard deviation, RSD in %) is also crucial to increase the precision of the calculated U-Pb ages. Fig. 8 shows how the uncertainty of the lower intercept U-Pb ages decreases with a greater spread in non-radiogenic Pb content. Using a power law trend, we calculated the maximum curvature point that intersects 0.29% of RSD above which the relative age uncertainty will drop under 3.1%. This relationship also suggests that a lower non-radiogenic Pb content lowers the relative uncertainty of calculated age (from low to high average nonradiogenic Pb content: FCT, BRA-1 and FCT titanites; Fig. 8). Thus, titanite U-Pb data with even a minor component of concordant or subconcordant U-Pb analyses led to the most precise age.

Several approaches can be used to optimize titanite U-Pb dating during a LA-ICP-MS session. This empirical estimate can feed several initiatives that propose real-time data reduction like 'GLITTER On-line analysis' for a commercial solution and the AgeCalcML freeware (Sundell et al., 2021). These real-time reduction solutions are key features to develop in routine in geochronology laboratories, specifically for nonradiogenic Pb rich mineral phases in order to optimize LA-ICP-MS sessions as well as to cluster statistically multiple titanite groups and associated tectonic events in detrital rock (see application and discussion in Bonamici and Blum, 2020). An alternative approach consists of screening/mapping titanite grains to (i) detect and prioritize concordant U-Pb data and (ii) to estimate the variability in non-radiogenic Pb content before running LA-ICP-MS analyses. Pre-screening titanite grains would allow to include concordant and near-concordant data during a LA-ICP-MS run and to strategically choose titanite spots to bring the largest variability in F207% with a single non-radiogenic Pb component and hence, minimize the calculated age uncertainty (see Fig. 8). This could be done using the U-Pb signal during pre-ablation (or cleaning) shots on grains.

Such very rapid U-Pb analyses have been conducted on zircons (Matthews and Guest, 2017; Sundell et al., 2021) and could be extended to the analysis of other grains to mitigate and monitor the non-radiogenic Pb content in Ti-rich accessory minerals.

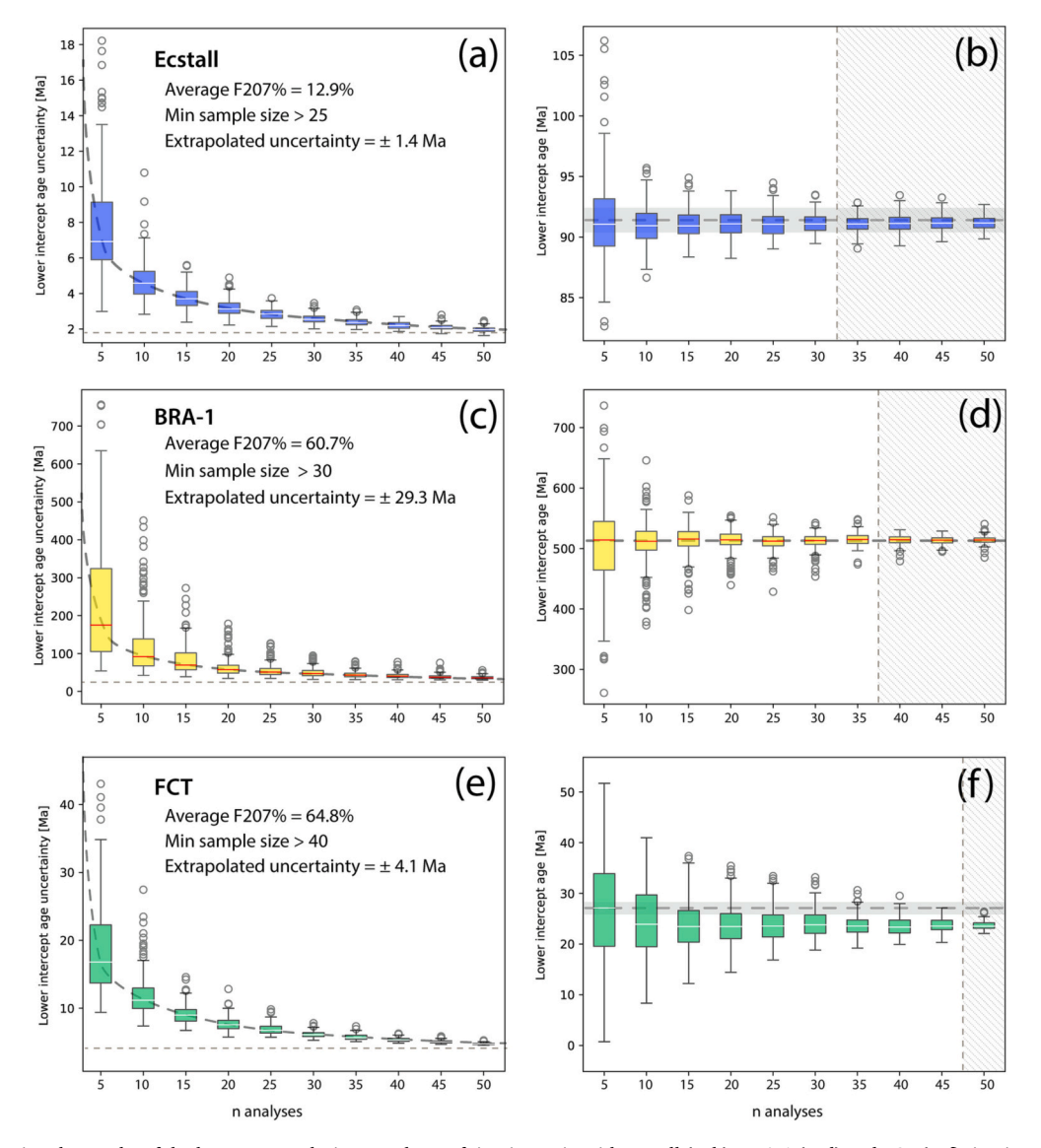


Fig. 7. Boxplots showing the results of the bootstrap analysis on each set of titanite grain with Ecstall (a; b), BRA-1 (c; d) and FCT (e; f) titanites. Left boxplot graphs show the evolution of age uncertainty with number of U—Pb analyses (i.e., precision) and right boxplot graphs show the evolution of calculated lower intercept ages with number of U—Pb analyses (i.e., accuracy).

5. Conclusion

In this contribution we present a comprehensive U-Pb, major and trace element dataset for five titanite reference materials: BLR-2, Ecstall, BRA-1, McClure and FCT (Table 3, Table 4 and Tables S1, S2 and S3), quantify the use of matrix-matched SRM for trace elements in titanite, and provide benchmarks for sample size necessary for dating non-radiogenic Pb rich phases. Based on our analysis we conclude:

- BLR-1 is a suitable primary SRM for determining titanite trace element concentrations. The use of BLR-1 yields a better overall reproducibility of trace element concentrations compared to NIST612, despite significantly overestimating Gd (PoD 25% 36%), Er (PoD 11% 21%) and Tm (PoD 12% 22%). Based on grain homogeneity, we propose BLR-2 titanite can also be used as a primary SRM for titanite to quantify trace element concentrations accurately and precisely. The Ecstall, McClure and FCT and BRA-1 grains are unsuited to serve as secondary reference materials given their higher chemical heterogeneity.
- The matrix-matched standardization approach (relative to BLR-1) with Si as the IES yields more accurate trace element

concentrations. However, this approach poorly reproduces Gd (PoD of 32.3%). Similarly, matrix-matched standardization with Ti as the IES yields accurate trace element concentrations. Both protocols yield similar results when the one-sample *t*-test is applied, generating statistically more significant trace element values than the other standardization techniques tested here. Moreover, the SQ standardization using BLR-1 as the SRM yielded a smaller weighted Pod, while also not having to characterize the grains via EMP for IES (Ca, Si or Ti) concentration determination prior to the LA-ICPMS analysis.

- The NIST612 standardization systematically underestimates trace element concentrations regardless of the IES used. Despite underestimation, the NIST612 Ca reduction yields overall reasonable results for more trace elements, with a few exceptions: U (PoD of 20.9%), Pb (PoD of –39.1%). The NIST612 standardization using Ti as the IES is not recommended for titanite trace element quantification since it consistently and significantly underestimates the elemental abundances.
- Titanite U-Pb lower intercept age spread, and associated uncertainties decrease with increasing sampling size (i.e., number of spot analyses) following a power law. Moreover, the uncertainty of the lower intercept U-Pb ages decreases with increasing range in

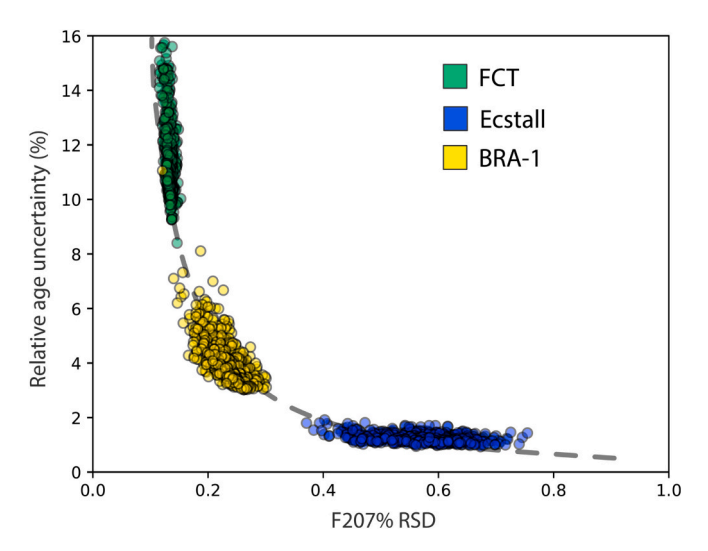


Fig. 8. Scatter plot showing the relationships between relative age uncertainty (in %) and the relative standard deviation of the non-radiogenic Pb content (F207%) for bootstrap runs (n > 30) of FCT, Ecstall and BRA-1 titanites.

non-radiogenic Pb contents, following a power law trend. The maximum curvature point of this trend points to 0.29% of RSD, above which the relative age uncertainty will drop under 3.1%. The empirical approach presented here can serve future analytical work through optimizing real-time data reduction towards more efficient data acquisitions and more robust U-Pb ages for non-radiogenic Pbrich phases.

Supplementary data to this article can be found online at https://doi.org/10.1016/j.chemgeo.2023.121635.

Declaration of Competing Interest

The authors declare that they have no known competing financial interests or personal relationships that could have appeared to influence the work reported in this paper.

Data availability

Data will be made available on request.

Acknowledgments

A.T. thanks the CNRS program as this research received funding from the program TelluS-SYSTER of the Institut National des Sciences de l'Univers, CNRS (the AIRCOO project). A.T. also acknowledges support from the Université Claude Bernard de Lyon with the "BQR Accueil EC 2022". M.N·D acknowledges grant C1.2.PFE-CDI.2021-587/ Contract no.41PFE/30.12.2021 from Romanian Ministry of Research, Innovation and Digitalization (MCID). This work was also supported by grants from the Romanian Executive Agency for Higher Education, Research, Development, and Innovation, UEFISCDI: PN-III-P4-PCE-2021-0901. We thank Derek Hoffman for his support in the clean lab, TIMS and ICP-MS laboratory at University of Arizona. We also thank I. GOBERT (Georessources, Nancy) for her help during trace element analyzes at the SARM laboratory. Matt Coble of Stanford University generously provided McClure reference material for analysis during this study. ALC analyses were supported by NSF-EAR 2050246. We thank editor Balz Kamber and three anonymous reviewers for valuable insights that helped us improve the manuscript.

References

Aleinikoff, J.N., Wintsch, R.P., Fanning, C.M., Dorais, M.J., 2002. U–Pb geochronology of zircon and polygenetic titanite from the Glastonbury Complex, Connecticut, USA: an integrated SEM, EMPA, TIMS, and SHRIMP study. Chem. Geol. 188 (1–2), 125–147.

Aleinikoff, J.N., Wintsch, R.P., Tollo, R.P., Unruh, D.M., Fanning, C.M., Schmitz, M.D., 2007. Ages and origins of rocks of the Killingworth dome, south-Central Connecticut: Implications for the tectonic evolution of southern New England. Am. J. Sci. 307 (1), 63–118.

Alexander Jr., E.C., 1979. MMhb-1: a new ⁴⁰Ar-³⁹Ar dating standard. Geochim. Cosmochim. Acta 43 (2), 278.

Barrat, J.A., Zanda, B., Moynier, F., Bollinger, C., Liorzou, C., Bayon, G., 2012.

Geochemistry of CI chondrites: Major and trace elements, and Cu and Zn isotopes.

Geochim. Cosmochim. Acta 83, 79–92.

Bonamici, C.E., Blum, T.B., 2020. Reconsidering initial Pb in titanite in the context of in situ dating. American Mineral: J. Farth Planet. Mater. 105 (11), 1672–1685.

Butler, R.F., Gehrels, G.E., Baldwin, S.E., Davidson, C., 2002. Paleomagnetism and geochronology of the Ecstall pluton in the Coast Mountains orogen of British Columbia: Local deformation rather than large-scale transport. J. Geophys. Res 107, 2009

Carignan, J., Hild, P., Mevelle, G., Morel, J., Yeghicheyan, D., 2001. Routine analyses of trace elements in geological samples using flow injection and low pressure on-line liquid chromatography coupled to ICP-MS: a study of geochemical reference materials BR, DR-N, UB-N, AN-G and GH. Geostand, Newslett. 25 (2–3), 187–198.

Chapman, J.B., Gehrels, G.E., Ducea, M.N., Giesler, N., Pullen, A., 2016. A new method for estimating parent rock trace element concentrations from zircon. Chem. Geol. 439, 59–70.

Chen, C.H., Hsieh, P.S., Wang, K.L., Yang, H.J., Lin, W., Liang, Y.H., Yang, H.C., 2010.Zircon LA-ICPMS U-Pb ages and Hf isotopes of Huayu (Penghu Islands) volcanics in the Taiwan Strait and tectonic implication. J. Asian Earth Sci. 37 (1), 17–30.

Cherniak, D.J., 1993. Lead diffusion in titanite and preliminary results on the effects of radiation damage on Pb transport. Chem. Geol. 110 (1–3), 177–194.

Chew, D.M., Sylvester, P.J., Tubrett, M.N., 2011. U–Pb and Th–Pb dating of apatite by LA-ICPMS. Chem. Geol. 280 (1–2), 200–216.

Chew, D.M., Petrus, J.A., Kamber, B.S., 2014. U-Pb LA-ICPMS dating using accessory mineral standards with variable common Pb. Chem. Geol. 363, 185–199.

Cioffi, C.R., Neto, M.D.C.C., Möller, A., Rocha, B.C., 2019. Titanite petrochronology of the southern Brasília Orogen basement: Effects of retrograde net-transfer reactions on titanite trace element compositions. Lithos 344, 393–408.

Ducea, M.N., Ganguly, J., Rosenberg, E.J., Patchett, P.J., Cheng, W., Isachsen, C., 2003. Sm-Nd dating of spatially controlled domains of garnet single crystals: a new method of high-temperature thermochronology. Earth Planet. Sci. Lett. 213 (1–2), 31–42.

Essex, R.M., Gromet, L.P., 2000. U-Pb dating of prograde and retrograde titanite growth during the Scandian orogeny. Geology 28 (5), 419–422.

Ferry, J.M., Watson, E.B., 2007. New thermodynamic models and revised calibrations for the Ti-in-zircon and Zr-in-rutile thermometers. Contrib. Mineral. Petrol. 154 (4), 429–437.

Frost, B.R., Chamberlain, K.R., Schumacher, J.C., 2001. Sphene (titanite): phase relations and role as a geochronometer. Chem. Geol. 172 (1–2), 131–148.

Fryer, B.J., Jackson, S.E., Longerich, H.P., 1995. The design, operation and role of the laser-ablation microprobe coupled with an inductively coupled plasma-mass spectrometer (LAM-ICP-MS) in the earth sciences. Can. Mineral. 33 (2), 303–312.

Gao, X.Y., Zheng, Y.F., Chen, Y.X., 2011. U–Pb ages and trace elements in metamorphic zircon and titanite from UHP eclogite in the Dabie orogen: constraints on P–T–t path. J. Metamorph. Geol. 29 (7), 721–740.

Gao, X.Y., Zheng, Y.F., Chen, Y.X., Guo, J., 2012. Geochemical and U–Pb age constraints on the occurrence of polygenetic titanites in UHP metagranite in the Dabie orogen. Lithos 136. 93–108.

Glorie, S., Jepson, G., Konopelko, D., Mirkamalov, R., Meeuws, F., Gilbert, S., De Grave, J., 2019. Thermochronological and geochemical footprints of post-orogenic fluid alteration recorded in apatite: implications for mineralisation in the Uzbek Tian Shan. Gondwana Res. 71. 1–15.

Hart-Madigan, L., Wilkinson, J.J., Lasalle, S., Armstrong, R.N., 2020. U-Pb dating of hydrothermal titanite resolves multiple phases of propylitic alteration in the Oyu Tolgoi porphyry district, Mongolia. Econ. Geol. 115 (8), 1605–1618.

Hayden, L.A., Watson, E.B., 2007. Rutile saturation in hydrous siliceous melts and its bearing on Ti-thermometry of quartz and zircon. Earth Planet. Sci. Lett. 258 (3–4), 561–568.

Hayden, L.A., Watson, E.B., Wark, D.A., 2008. A thermobarometer for sphene (titanite). Contrib. Mineral. Petrol. 155 (4), 529–540.

He, D., Liu, Y., Tong, X., Zong, K., Hu, Z., Gao, S., 2013. Multiple exsolutions in a rare clinopyroxene megacryst from the Hannuoba basalt, North China: Implications for subducted slab-related crustal thickening and recycling. Lithos 177, 136–147.

Hewitt, D.F., Thomson, J.E., 1956. The Grenville region of Ontario. *The Grenville*. P~roblem, pp. 22–41.

Horstwood, M.S., Košler, J., Gehrels, G., Jackson, S.E., McLean, N.M., Paton, C., Schoene, B., 2016. Community-derived standards for LA-ICP-MS U-(Th-) Pb geochronology-uncertainty propagation, age interpretation and data reporting. Geostand. Geoanal. Res. 40 (3), 311–332.

Hutchison, W.W., 1982. Geology of the Prince Rupert-Skeena map area, British Columbia. Geol. Surv. Canada 394.

Jepson, G., Carrapa, B., George, S.W., Triantafyllou, A., Egan, S.M., Constenius, K.N., Ducea, M.N., 2021. Resolving mid-to upper-crustal exhumation through apatite petrochronology and thermochronology. Chem. Geol. 565, 120071.

- Kirkland, C.L., Hollis, J., Danišík, M., Petersen, J., Evans, N.J., McDonald, B.J., 2017. Apatite and titanite from the Karrat Group, Greenland; implications for charting the thermal evolution of crust from the U-Pb geochronology of common Pb bearing phases. Precambrian Res. 300, 107–120.
- Kirkland, C.L., Fougerouse, D., Reddy, S.M., Hollis, J., Saxey, D.W., 2018. Assessing the mechanisms of common Pb incorporation into titanite. Chem. Geol. 483, 558–566.
- Kirkland, C.L., Yakymchuk, C., Gardiner, N.J., Szilas, K., Hollis, J., Olierook, H., Steenfelt, A., 2020. Titanite petrochronology linked to phase equilibrium modelling constrains tectono-thermal events in the Akia Terrane, West Greenland. Chem. Geol. 536, 119467.
- Kohn, M.J., 2017. Titanite petrochronology. Rev. Mineral. Geochem. 83 (1), 419–441.
 Kohn, M.J., Corrie, S.L., 2011. Preserved Zr-temperatures and U–Pb ages in high-grade metamorphic titanite: evidence for a static hot channel in the Himalayan orogen. Earth Planet. Sci. Lett. 311 (1–2), 136–143.
- Kylander-Clark, A.R., Hacker, B.R., Cottle, J.M., 2013. Laser-ablation split-stream ICP petrochronology. Chem. Geol. 345, 99–112.
- Li, X.H., Liang, X., Sun, M., Liu, Y., Tu, X., 2000. Geochronology and geochemistry of single-grain zircons: Simultaneous in-situ analysis of U-Pb age and trace elements by LAM-ICP-MS. Eur. J. Mineral. 12 (5), 1015–1024.
- Liu, Y., Hu, Z., Gao, S., Günther, D., Xu, J., Gao, C., Chen, H., 2008. In situ analysis of major and trace elements of anhydrous minerals by LA-ICP-MS without applying an internal standard. Chem. Geol. 257 (1–2), 34–43.
- Liu, T., Jiang, S.Y., Zheng, R.H., Chen, W., 2022. Titanite U-Pb dating and geochemical constraints on the Paleozoic magmatic-metamorphic events and Nb-Ta mineralization in the Yushishan deposit, South Qilian, NW China. Lithos 412, 106612
- Ma, Q., Evans, N.J., Ling, X.X., Yang, J.H., Wu, F.Y., Zhao, Z.D., Yang, Y.H., 2019. Natural titanite reference materials for in situ U-Pb and Sm-Nd isotopic measurements by LA-(MC)-ICP-MS. Geostand. Geoanal. Res. 43 (3), 355–384.
- Matthews, W.A., Guest, B., 2017. A practical approach for collecting large-n detrital zircon U-Pb data sets by quadrupole LA-ICP-MS. Geostand. Geoanal. Res. 41 (2), 161–180.
- Mazdab, F.K., 2009. Characterization of flux-grown trace-element-doped titanite using the high-mass-resolution ion microprobe (SHRIMP-RG). Can. Mineral. 47 (4), 813–831.
- Mcclelland, W.C., Gilotti, J.A., Mazdab, F.K., Wooden, J.L., 2009. Trace-element record in zircons during exhumation from UH P conditions, North-East Greenland Caledonides. Eur. J. Mineral. 21 (6), 1135–1148.
- Miliszkiewicz, N., Walas, S., Tobiasz, A., 2015. Current approaches to calibration of LA-ICP-MS analysis. J. Anal. At. Spectrom. 30 (2), 327–338.
- Moser, A.C., Hacker, B.R., Gehrels, G.E., Seward, G.G., Kylander-Clark, A.R., Garber, J. M., 2022. Linking titanite U-Pb dates to coupled deformation and dissolution reprecipitation. Contrib. Mineral. Petrol. 177 (3), 1–27.
- Mottram, C.M., Cottle, J.M., Kylander-Clark, A.R., 2019. Campaign-style U-Pb titanite petrochronology: along-strike variations in timing of metamorphism in the Himalayan metamorphic core. Geosci. Front. 10 (3), 827–847.
- Nakada, S., 1991. Magmatic processes in titanite-bearing dacites, Central Andes of Chile and Bolivia. Am. Mineral. 76 (3-4), 548-560.
- Olierook, H.K., Taylor, R.J., Erickson, T.M., Clark, C., Reddy, S.M., Kirkland, C.L., Barham, M., 2019. Unravelling complex geologic histories using U–Pb and trace element systematics of titanite. Chem. Geol. 504, 105–122.
- Olson, J.C., Marvin, R.F., Parker, R.L., Mehnert, H.H., 1977. Age and tectonic setting of lower Paleozoic alkalic and mafic rocks, carbonatites, and thorium veins in south-Central Colorado. US Geol. Surv. J. Res. 5 (6), 673–687.
- Pan, L.C., Hu, R.Z., Bi, X.W., Li, C., Wang, X.S., Zhu, J.J., 2018. Titanite major and trace element compositions as petrogenetic and metallogenic indicators of Mo ore deposits: examples from four granite plutons in the southern Yidun arc, SW China. American Mineral.: J. Earth Planet. Mater. 103 (9), 1417–1434.
- Papapavlou, K., Darling, J.R., Lightfoot, P.C., Lasalle, S., Gibson, L., Storey, C.D., Moser, D., 2018. Polyorogenic reworking of ore-controlling shear zones at the South Range of the Sudbury impact structure: A telltale story from in situ U–Pb titanite geochronology. Terra Nova 30 (3), 254–261.
- Paton, C., Hellstrom, J., Paul, B., Woodhead, J., Hergt, J., 2011. Iolite: Freeware for the visualisation and processing of mass spectrometric data. J. Anal. At. Spectrom. 26 (12), 2508–2518.
- Petrus, J.A., Kamber, B.S., 2012. VizualAge: a novel approach to laser ablation ICP-MS U-Pb geochronology data reduction. Geostand. Geoanal. Res. 36 (3), 247–270.
- Pullen, A., Ibáñez-Mejia, M., Gehrels, G.E., Giesler, D., Pecha, M., 2018. Optimization of a laser ablation-single collector-inductively coupled plasma-mass spectrometer (Thermo Element 2) for accurate, precise, and efficient zircon U-Th-Pb geochronology. Geochem. Geophys. Geosyst. 19 (10), 3689–3705.

Schmitz, M.D., Bowring, S.A., 2001. U-Pb zircon and titanite systematics of the fish Canyon Tuff: an assessment of high-precision U-Pb geochronology and its application to young volcanic rocks. Geochim. Cosmochim. Acta 65 (15), 2571–2587.

- Schoene, B., Bowring, S.A., 2006. U–Pb systematics of the McClure Mountain syenite: thermochronological constraints on the age of the 40Ar/39Ar standard MMhb. Contrib. Mineral. Petrol. 151 (5), 615–630.
- Schwartz, J.J., Stowell, H.H., Klepeis, K.A., Tulloch, A.J., Kylander-Clark, A.R., Hacker, B.R., Coble, M.A., 2016. Thermochronology of extensional orogenic collapse in the deep crust of Zealandia. Geosphere 12 (3), 647–677.
- Scibiorski, E.A., Cawood, P.A., 2022. Titanite as a petrogenetic indicator. Terra Nova 34
- Scibiorski, E., Kirkland, C.L., Kemp, A.I.S., Tohver, E., Evans, N.J., 2019. Trace elements in titanite: a potential tool to constrain polygenetic growth processes and timing. Chem. Geol. 509, 1–19.
- Simonetti, A., Heaman, L.M., Chacko, T., Banerjee, N.R., 2006. In situ petrographic thin section U–Pb dating of zircon, monazite, and titanite using laser ablation–MC–ICP–MS. Int. J. Mass Spectrom. 253 (1–2), 87–97.
- Smith, A.L., 1970. Sphene, perovskite and coexisting Fe-Ti oxide minerals. American Mineral.: J. Earth Planet. Mater. 55 (1–2), 264–269.
- Smye, A.J., Marsh, J.H., Vermeesch, P., Garber, J.M., Stockli, D.F., 2018. Applications and limitations of U-Pb thermochronology to middle and lower crustal thermal histories. Chem. Geol. 494, 1–18.
- Song, S., Mao, J., Xie, G., Chen, L., Santosh, M., Chen, G., Ouyang, Y., 2019. In situ LA-ICP-MS U-Pb geochronology and trace element analysis of hydrothermal titanite from the giant Zhuxi W (Cu) skarn deposit, South China. Mineral. Deposita 54 (4), 569-590.
- Spandler, C., Hammerli, J., Sha, P., Hilbert-Wolf, H., Hu, Y., Roberts, E., Schmitz, M., 2016. MKED1: a new titanite standard for in situ analysis of Sm–Nd isotopes and U–Pb geochronology. Chem. Geol. 425, 110–126.
- Spencer, K.J., Hacker, B.R., Kylander-Clark, A.R.C., Andersen, T.B., Cottle, J.M., Stearns, M.A., Seward, G.G.E., 2013. Campaign-style titanite U-Pb dating by laser-ablation ICP: Implications for crustal flow, phase transformations and titanite closure. Chem. Geol. 341, 84-101.
- Stearns, M.A., Hacker, B.R., Ratschbacher, L., Rutte, D., Kylander-Clark, A.R.C., 2015. Titanite petrochronology of the Pamir gneiss domes: Implications for middle to deep crust exhumation and titanite closure to Pb and Zr diffusion. Tectonics 34 (4), 784–802.
- Stearns, M.A., Cottle, J.M., Hacker, B.R., Kylander-Clark, A.R.C., 2016. Extracting thermal histories from the near-rim zoning in titanite using coupled U-Pb and traceelement depth profiles by single-shot laser-ablation split stream (SS-LASS) ICP-MS. Chem. Geol. 422, 13–24.
- Storey, C.D., Jeffries, T.E., Smith, M., 2006. Common lead-corrected laser ablation ICP–MS U–Pb systematics and geochronology of titanite. Chem. Geol. 227 (1–2), 37–52.
- Sundell, K.E., Gehrels, G.E., Pecha, M.E., 2021. Rapid U-Pb geochronology by laser ablation multi-collector ICP-MS. Geostand. Geoanal. Res. 45 (1), 37–57.
- Tiepolo, M., Oberti, R., Vannucci, R., 2002. Trace-element incorporation in titanite: constraints from experimentally determined solid/liquid partition coefficients. Chem. Geol. 191 (1–3), 105–119.
- Timms, N.E., Kinny, P.D., Reddy, S.M., Evans, K., Clark, C., Healy, D., 2011. Relationship among titanium, rare earth elements, U–Pb ages and deformation microstructures in zircon: Implications for Ti-in-zircon thermometry. Chem. Geol. 280 (1–2), 33–46.
- Tomkins, H.S., Powell, R., Ellis, D.J., 2007. The pressure dependence of the zirconium-in-rutile thermometer. J. Metamorph. Geol. 25 (6), 703–713.
- Ubide, T., McKenna, C.A., Chew, D.M., Kamber, B.S., 2015. High-resolution LA-ICP-MS trace element mapping of igneous minerals: in search of magma histories. Chem. Geol. 409, 157–168.
- Vermeesch, P., 2018. IsoplotR: a free and open toolbox for geochronology. Geosci. Front. 9 (5), 1479–1493.
- Walters, J.B., Cruz-Uribe, A.M., Song, W.J., Gerbi, C., Biela, K., 2022. Strengths and limitations of in situ U–Pb titanite petrochronology in polymetamorphic rocks: An example from western Maine, USA. J. Metamorph. Geol. 40 (6), 1043–1066.
- Whitney, J.A., Stormer, J.R., J. C., 1985. Mineralogy, petrology, and magmatic conditions from the fish Canyon Tuff, Central San Juan volcanic field, Colorado. J. Petrol. 26 (3), 726–762.
- Zack, T., Moraes, R.D., Kronz, A., 2004. Temperature dependence of Zr in rutile: empirical calibration of a rutile thermometer. Contrib. Mineral. Petrol. 148 (4), 471–488.